Mitochondrial phenotypes in purified human immune cell subtypes and cell mixtures

Shannon Rausser[1], Caroline Trumpff[1], Marlon A McGill[1], Alex Junker[1], Wei Wang[2], Siu-hong Ho[2], Anika Mitchell[1], Kalpita R Karan[1], Catherine Monk[1,6,7], Suzanne C. Segerstrom[3], Rebecca G. Reed[4], Martin Picard[1,5,7]

[1] Department of Psychiatry, Division of Behavioral Medicine, Columbia University Irving Medical Center, New York, NY 10032, USA

[2] Columbia Center for Translational Immunology, Columbia University Irving Medical Center, New York, NY 10032, USA

[3] Department of Psychology, University of Kentucky, Lexington, KY, 40506, USA

[4] Department of Psychology, University of Pittsburgh, Pittsburgh, PA, 15260, USA

[5] Department of Neurology, Merritt Center, Columbia University Irving Medical Center, New York, NY 10032, USA

[6] Department of Obstetrics & Gynecology, Columbia University Irving Medical Center, New York, NY 10032, USA

[7] New York State Psychiatric Institute, New York, NY 10032, USA

Correspondence: martin.picard@columbia.edu

Abstract: Using a high-throughput mitochondrial phenotyping platform to quantify multiple mitochondrial features among immunologically-defined immune cell subtypes, we define the natural variation in mitochondrial content, mitochondrial DNA copy number (mtDNAcn), and respiratory chain enzymatic activities in human neutrophils, monocytes, B cells, naïve and memory T lymphocyte subtypes. In mixed peripheral blood mononuclear cells (PBMCs) from the same individuals, we show how mitochondrial measures are confounded by both cell type distributions and contaminating platelets. Cell subtype-specific measures among women and men spanning 4 decades of life indicates age- and sex-related differences, including an age-related elevation in mitochondrial DNA copy number (mtDNAcn), which are masked or blunted in mixed PBMCs. Finally, a proof-of-concept, repeated-measures study in a single individual validates cell type differences and also reveals week-to-week changes in mitochondrial activities. Together, these mitochondrial phenotype data in defined circulating human leukocytes sub-populations provide foundational knowledge to develop interpretable blood-based assays of mitochondrial health.

Keywords: mitochondria; leukocytes; sexual dimorphism; aging; dynamic variation

Mitochondria are the most studied organelle across biomedical sciences[1]. Mitochondrial (dys)function may affect disease risk and aging[1-3] and mediate psycho-biological processes[4]. Tractable quantitative biomarkers and mitochondrial content (the mass of mitochondria per cell) and function (energy production capacity) in accessible human tissues, such as peripheral blood leukocytes, are needed. Cell-specific assays can interrogate mitochondrial function in immune cells[5], but more frequently used assays of peripheral blood mononuclear cells (PBMCs)[6-11] assume that the immunometabolic properties of different immune cells have a negligible effect. Mitochondrial measurements in PBMCs may be confounded by biological factors such as: i) cell type composition, ii) platelet contamination, iii) mitochondrial properties across different immune cells, and iv) the variability of cell type composition and bioenergetics over time. These four main gaps in knowledge limit our understanding on whether quantifying mitochondrial function in observational and intervention studies requires purified cell populations.

Immune cell subtypes are normally mobilized from lymphoid organs into circulation in a diurnal fashion and with acute stress[12-15], substantially influencing the pool of peripheral blood leukocyte composition. Moreover, circulating immune cell subtypes vary extensively between individuals, partially attributable to both individual-level (e.g., sex and age) and environmental factors[16]. As a result, whole blood and PBMCs from different individuals reflect different cell populations, with mixed lymphocytes and monocytes particularly differing in their respiratory properties and mitochondrial respiratory chain (RC) protein abundance[5, 17, 18 19]. Therefore, we hypothesized that the relative abundance of different cell types (i.e., cell type composition) confounds measurements of PBMC mitochondrial functions. Furthermore, Ficoll-isolated PBMCs are contaminated with (sticky) platelets[20]. Platelets contain mitochondria and mtDNA but no nuclear genome to use as reference for mtDNA copy number (mtDNAcn) measurements[21], adding another source of bias to mitochondrial studies in PBMCs or other undefined cell mixtures[22-24]. Developing biologically valid measures of mitochondrial health requires quantifying the influence of cell type abundance and platelet contamination, enabling scalable translational mitochondrial research on specific features of mitochondrial biology.

Mitochondria are multifunctional organelles for which content and function vary based on the tissue and cell type they inhabit[25, 26], a phenomenon termed functional specialization[27]. Within specific molecularly-defined immune cell subtypes, there is little known about the nature and

magnitude of differences in mitochondrial phenotypes. But in the immune system, the acquisition of specialized cellular characteristics during differentiation is determined by changes in mitochondrial metabolism[28]. For example, the activation, proliferation, and differentiation of both monocytes[29] and T cells[30] into specific effector cells require distinct metabolic profiles and cannot proceed without the proper metabolic states. Likewise, naïve and memory T lymphocytes differ in their reliance on mitochondrial oxidative phosphorylation (OXPHOS) involving the RC enzymes[31-33], and harbor differences in protein composition and mitochondrial content within the cytoplasm[34]. Thus, we hypothesized that circulating immune cell subtypes in human blood should exhibit robust differences in mitochondrial phenotypes (mitotypes) including both features of mitochondrial content and RC enzymatic activities.

An equally significant gap in knowledge relates to the natural dynamic variation in mitochondrial content and function. Mitochondria dynamically recalibrate in response to stress exposure (for a review see[35]), and well-defined mitochondrial recalibrations to stress[35] and exercise[36] suggest that cell-specific mitochondrial features could vary over time. Are leukocyte mitochondrial content and RC function stable *trait*-like properties of each person, or are they *state*-like features, possibly varying in response to metabolic or endocrine mediators?

To address these questions, we used a high-throughput mitochondrial phenotyping platform on immunologically-defined immune cell subtypes, in parallel with PBMCs, to define cell-specific, multivariate mitochondrial phenotypes[10]. First, we establish the extent to which cell type composition and platelet contamination influence PBMCs-based mitochondrial measures. We then systematically map the mitochondrial properties of different immune cell subtypes and validate the existence of stable mitochondrial phenotypes in an intensive repeated-measures design within the same individual, which begins to reveal a surprising degree of change over time. Collectively, these data highlight the limitations of PBMCs to profile human mitochondrial function between individuals and over time, and define unique cell-specific mitochondrial features in circulating human leukocytes in relation to age, sex, and biomarkers. These data represent a resource to design cell-specific immune mitochondrial phenotyping strategies in future studies.

Results

Cell subtype distributions by age and sex

We performed mitochondrial profiling on molecularly-defined subtypes of immune cell populations in parallel with PBMCs in twenty one participants (11 women, 10 men) distributed across 4 decades of life (ages 20-59, 4-8 participants per decade across both sexes). From each participant, 100ml of blood was collected; total leukocytes were then labeled with two cell surface marker cocktails, counted, and isolated by fluorescence-activated cell sorting (FACS, see Methods for details), and processed on our mitochondrial phenotyping platform adapted from[10] (Figure 1a). In parallel, a complete blood count (CBC) for the major leukocyte populations in whole blood, standard blood chemistry, and a metabolic and endocrine panel were assessed (Figure 1b).

We first quantified the abundance of specific cell subtypes based on cell surface marker combinations (Figure 1c, Supplemental Figures 1-2, and Supplemental Table 1). Men had on average 35-44% more NK cells and monocytes but 66% fewer $CD4^+$ naïve T cells than women (Figure 1d). These differences were characterized by moderate to large standardized effect sizes (Hedges' g=0.71-0.93). Between individuals of the same sex, the circulating proportions of various cell subtypes (e.g., B cells range: <0.01-15.3%, see Supplemental Table 2) varied by up to an order of magnitude (i.e., 10-fold) (Figure 1e).

In relation to age, as expected[16], $CD8^+$ naïve T cells abundance was lower in older individuals ($p<0.01$). Compared to young adults in their 20's, middle-aged individuals in their 50's had on average ~63% fewer $CD8^+$ naïve T cells (Figure 1f). In contrast, memory $CD4^+$ EM and $CD8^+$ CM abundance tended to increase in abundance with age (positive correlation, r=0.31 for both), an overall picture consistent with immunological aging[16, 37].

CBC-derived cell proportions also showed that men had on average 28% more monocytes than women (Supplemental Figure 3), consistent with our FACS results. Conversely, women had on average 20% more platelets than men. Platelet abundance also tended to decrease with age, a point discussed later.

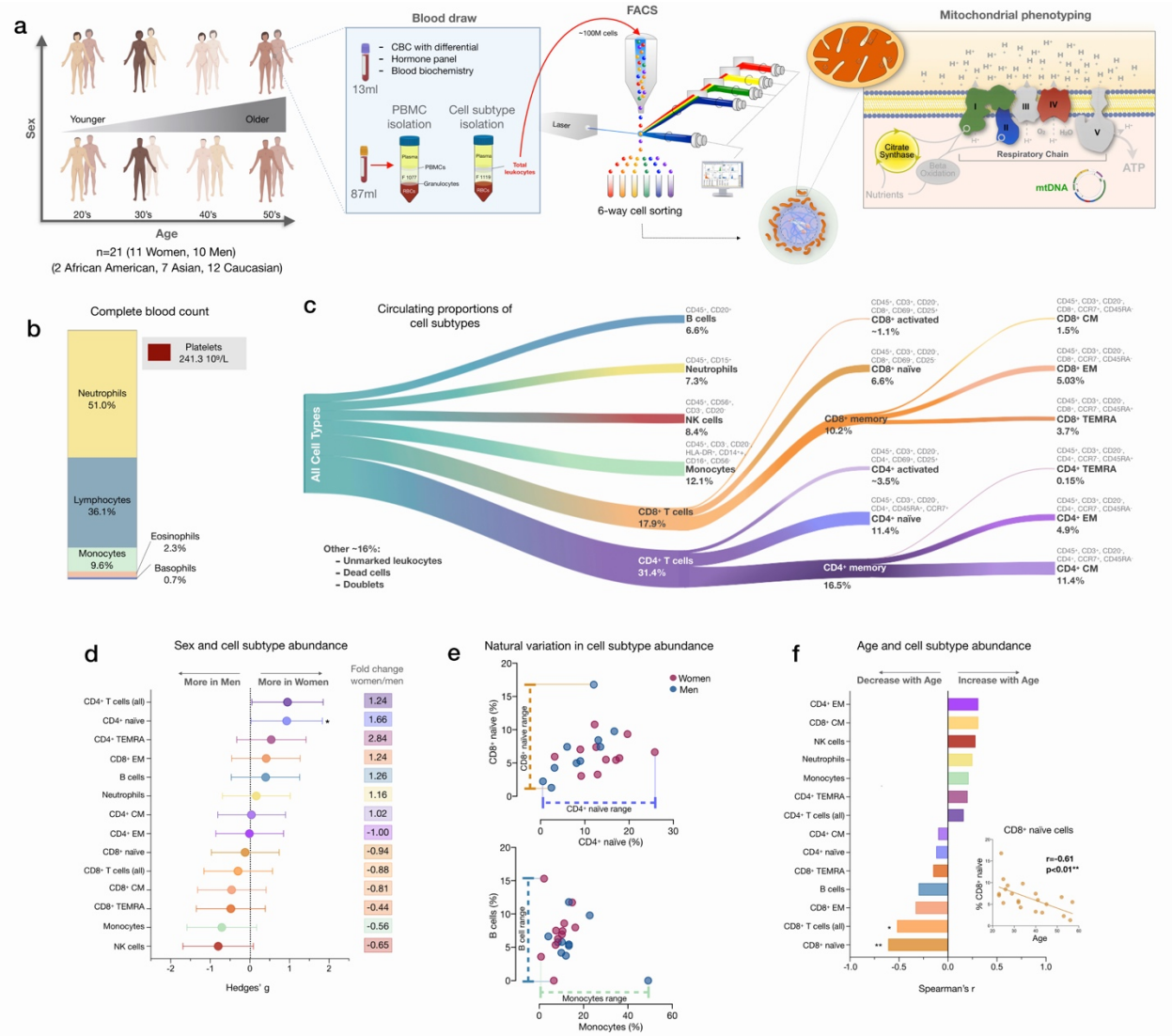

Figure 1 – Immune cell subtype distribution in adult women and men. (**a**) Overview of participant demographics, blood collection, processing, and analysis pipeline. Total leukocytes were isolated using Ficoll 1119 and PBMCs were isolated on Ficoll 1077. (*right*) The five mitochondrial features analyzed on the mitochondrial phenotyping platform are colored. Mitochondrial phenotyping platform schematic adapted from[10]. (**b**) Stacked histogram showing the leukocytes distribution derived from the complete blood count (CBC) of major cell types. (**c**) Diagram illustrating the proportion of circulating immune cell subtypes (% of all detected cells) quantified by flow cytometry from total peripheral blood leukocytes. Cell surface markers and subtype definitions are detailed in Supplemental Table 1. (**d**) Effect sizes for cell subtype distribution differences between women (n=11) and men (n=10). P-values from non-parametric Mann-Whitney T test. Error bars reflect the 95% confidence interval (C.I.) on the effect size, and the fold change comparing raw counts between women and men is shown on the right. (**e**) Example distributions of cell type proportions in women and men illustrating the range of $CD4^+$ and $CD8^+$ naïve cells, B cells, and monocytes, highlighting the natural variation among our cohort. Each datapoint reflects a different individual. (**f**) Spearman's r correlation between age and cell types proportion. n=21, $p<0.05$*, $p<0.01$**.

Circulating cell composition influence PBMCs mitochondrial phenotypes

We next examined how much the abundance of various circulating immune cell subtypes correlates with individual mitochondrial metrics in PBMCs. Our analysis focused on two key aspects of mitochondrial biology: i) *mitochondrial content*, indexed by citrate synthase (CS) activity, a Kreb's cycle enzyme used as a marker of mitochondrial volume density[38], and mtDNAcn, reflecting the number of mtDNA copies per cell; and ii) *RC function* measured by complex I (CI), complex II (CII) and complex IV (CIV) enzymatic activities, which reflect the capacity for electron transport and respiratory capacity and serve here as a proxy for maximal RC capacity. Furthermore, by adding the three mean-centered features of RC function together as a numerator (CI+CII+CIV), and dividing this by the combination of content features (CS+mtDNAcn), we obtained an index reflecting *RC capacity on a per-mitochondrion basis*, known as the mitochondrial health index (MHI) adapted from previous work[10].

As expected, the abundance of multiple circulating cells was correlated with PBMCs mitochondrial features (Figure 2). Notably, the proportion of circulating B cells accounted for 27% of the variance (r^2) in PBMCs mtDNAcn, and for 32-61% of the variance in CS, CI, and CII activities. The proportion of other cell types accounted for more modest portions (<14%) of the variance in PBMCs, although the higher abundance of memory cells tended to be negatively associated with PBMCs RC enzymatic activities.

Based on CBC-derived cell proportions, the abundance of eosinophils and neutrophils was positively correlated with most PBMCs mitochondrial content and activity features (Supplemental Figure 4a). Because PBMCs do not contain granulocytes, these correlations may reflect the independent effect of a humoral factor on cell mobilization and mitochondrial function. Together, these data demonstrate that mitochondrial features assessed in PBMCs in part reflect the proportions of some but not all circulating cell subtypes, objectively documenting cell type distribution as a confounding factor in the measurements of mitochondrial function in PBMCs.

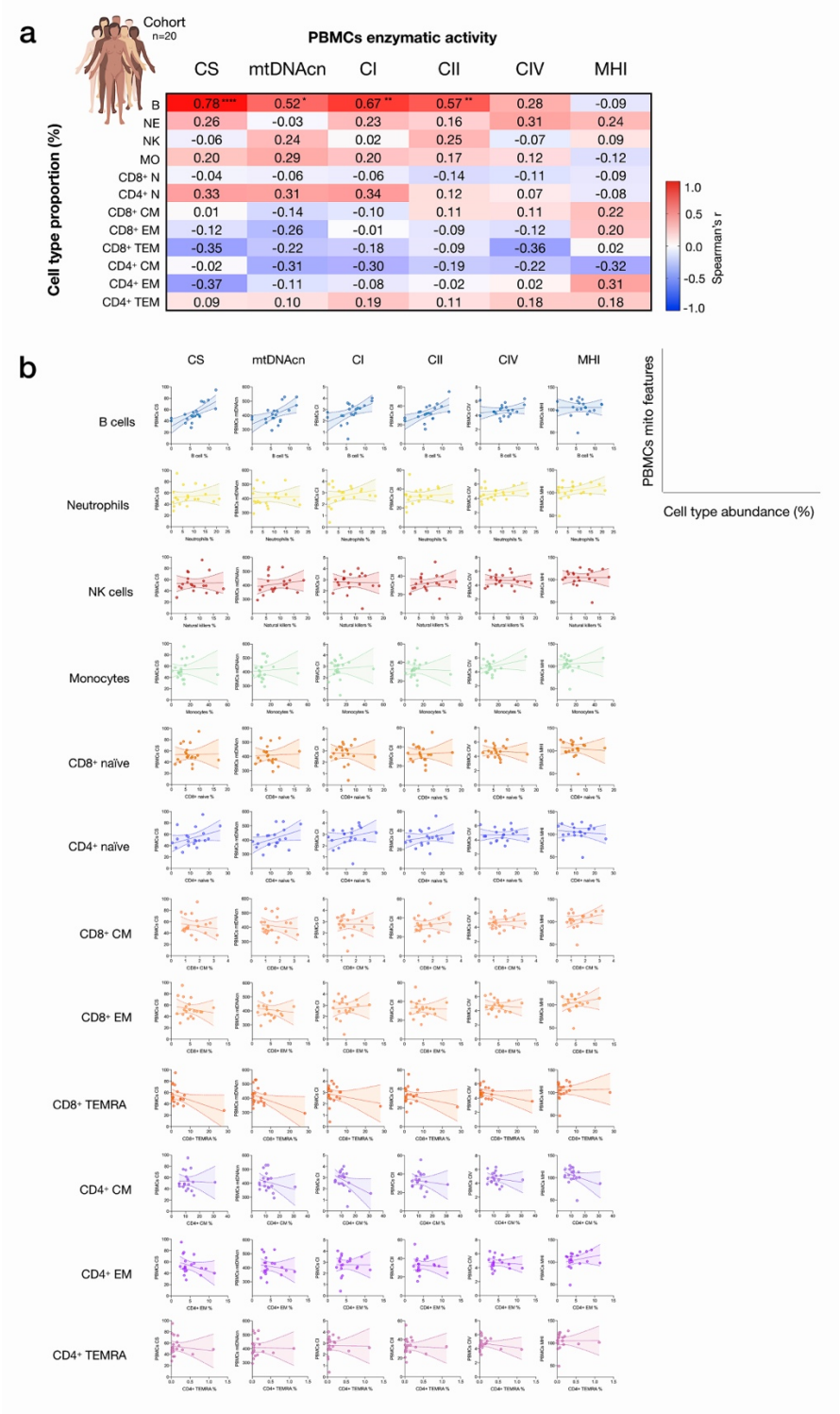

Figure 2 – Influence of cell subtypes on mitochondrial features in total PBMCs. (**a**) Pairwise correlations (Spearman's r) between cell subtype proportions obtained from cell sorting with mitochondrial features measured in PBMCs for the cohort (n=20). Aggregate correlations are shown as a heatmap (*top*) and (**b**) individual scatterplots (*bottom*).

Platelets influence PBMCs mitochondrial phenotypes

Given that platelets easily form platelet-leukocyte aggregates[20] (Figure 3a), to partly resolve the origin of the discrepancies between isolated cell subtypes and PBMCs noted above, we directly quantified the contribution of platelets to total mitochondrial content and activity features in PBMCs. We note that the PBMCs in our experiments were carefully prepared with two passive platelet depletion steps (low speed centrifugations, see *Supplemental Methods* for details).

We first asked if the abundance of platelets from the CBC data in the cohort varies by age. Consistent with two large epidemiological studies of >40,000 individuals[39, 40], we found that platelet count decreased by ~6% for each decade of life (Figure 3b-c). This reflects a decline of 24% between the ages of 20 and 60, although the effect sizes vary by cohort and our estimate is likely overestimated due to the small size of our cohort. As expected, total blood platelet count tended to be consistently *positively* correlated with mtDNAcn, CS and RC activities in PBMCs (r=0.031-0.38) (Figure 3d). Therefore, the age-related loss of platelets and of the mtDNA contained within them could account for the previously reported age-related decline in mtDNAcn from studies using either whole blood[41, 42] (which includes all platelets) or PBMCs[43] (which include fewer contaminating platelets).

We directly tested this hypothesis by immunodepleting platelets from "clean" PBMCs and comparing three resulting fractions: total PBMCs, active platelet-depleted PBMCs, and platelet-enriched eluate. As expected, platelet depletion decreased mtDNAcn, CS, and RC activities, indicating that contaminating platelets exaggerated specific mitochondrial features by 9-22%, with the exception of complex IV (Figure 3f). Moreover, the platelet-enriched eluate showed 23-100% higher mitochondrial activities relative to total PBMCs, providing direct evidence that our platelet depletion method was effective and that platelets inflate estimates of mitochondrial abundance and RC activity in standard PBMCs. Interestingly, the composite MHI was minimally affected by the platelet depletion procedure, suggesting that this multivariate index of respiratory chain capacity on a per-mitochondrion basis may be more robust to platelet contamination than its individual features.

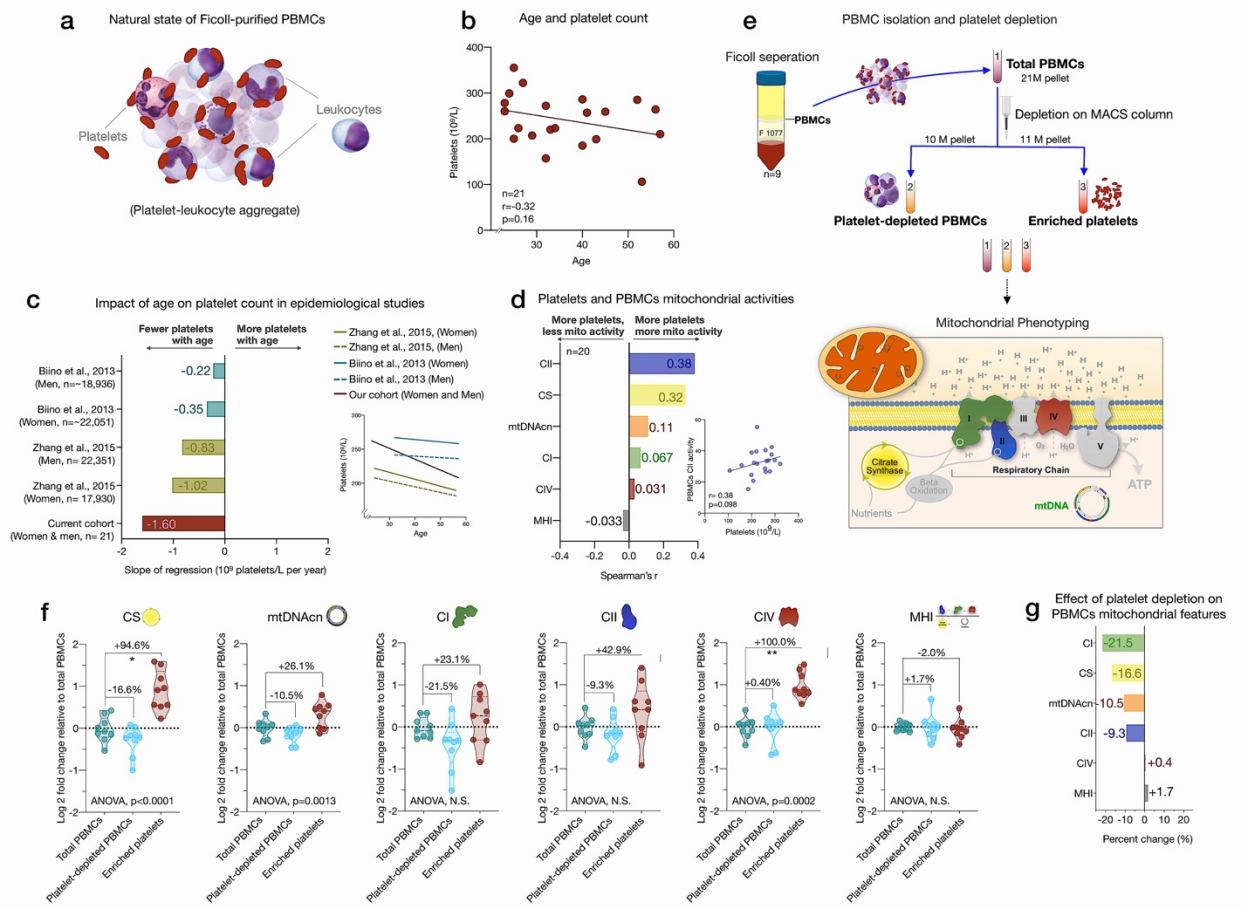

Figure 3 – Influence of platelet contamination on mitochondrial features in total PBMCs. (**a**) Schematic of the natural state of Ficoll-isolated PBMCs associated with contaminating platelets. (**b**) Association of age and circulating platelet abundance (i.e., count) in our cohort (Spearman's r). (**c**) Change in platelet abundance as a function of age. The magnitude of the association (slope of the regression: 109 platelets/L per year) from two large epidemiological studies and our cohort. The inset shows the actual regressions (n=21 to 22,351). (**d**) Effect sizes of the association between platelet count and PBMCs mitochondrial features in our cohort (n=20). (**e**) Overview of the experimental PBMC platelet depletion study, yielding three different samples subjected to mitochondrial phenotyping. Mitochondrial phenotyping platform schematic adapted from[10]. (**f**) Fold change in mitochondrial parameters between i) platelet-depleted PBMCs, and ii) enriched platelets (with contaminating PBMCs), relative to iii) total PBMCs. P-values from One-Way non-parametric ANOVA Friedman test, post-hoc Dunn's multiple comparisons relative to total PBMCs. (**g**) Percent change of platelet-depleted PBMCs mitochondrial features from total PBMCs. n=9, $p<0.05$*, $p<0.01$**, $p<0.001$***, $p<0.0001$****.

Individual cell subtypes are biologically distinct from PBMCs

Mitochondria phenotyping was performed in FACS-purified immune cells, in parallel with PBMCs. To obtain sufficient numbers of cells for mitochondrial phenotyping, we selected the 6 most abundant cell subtypes for each individual and isolated $5x10^6$ cells for each sample. Because

memory subtypes were relatively rare, central and effector memory (CM and EM) subtypes were pooled for $CD4^+$ and/or $CD8^+$ (CM-EM). This generated a total of 340 biological samples, including 136 biological replicates, yielding 204 individual participant/cell subtype combinations used for mitochondrial phenotyping.

Among cell subtypes, CS activity was highest in monocytes and B cells, and lowest in $CD4^+$ naïve T cells, with other cell types exhibiting intermediate levels (Figure 4a). Regarding mitochondrial genome content, B cells had the highest mtDNAcn with an average 451 copies per cell compared to neutrophils and NK cells, which contained only an average of 128 ($g=5.94$, $p<0.0001$) and 205 copies ($g=3.84$, $p<0.0001$) per cell, respectively (Figure 4b). Naïve and memory $CD4^+$ and $CD8^+$ T lymphocytes had intermediate mtDNAcn levels of ~300 copies per cell, with the exception of $CD8^+$ naïve cells (average of 427 copies per cell). Between cell types, CS activity and mtDNAcn differed by up to 3.52-fold.

In relation to RC function, monocytes had the highest Complexes I, II, and IV activities. Consistent with their low mtDNAcn, neutrophils also had the lowest activities across complexes, whereas naïve and memory subtypes of T and B lymphocytes presented intermediate RC enzyme activities (Figure 4c-e). PBMCs had up to 2.9-fold higher levels of CS, CI, and CII activity per cell than any of the individual cell subtypes measured, again consistent with platelet contamination.

The correlations between different mitochondrial features indicate that CS and mtDNAcn were only weakly correlated with each other, and in some cases were negatively correlated (Figure 4f). For RC complexes CI, CII, and CIV, which physically interact and whose function is synergistic within the inner mitochondrial membrane, correlations tended to be positive, as expected (Figure 4f). However, relatively weak and absent inter-correlations between mitochondrial features in some cell types reveal that each metric (i.e., content features and enzymatic activities) provides relatively independent information about the immune cell mitochondrial phenotype.

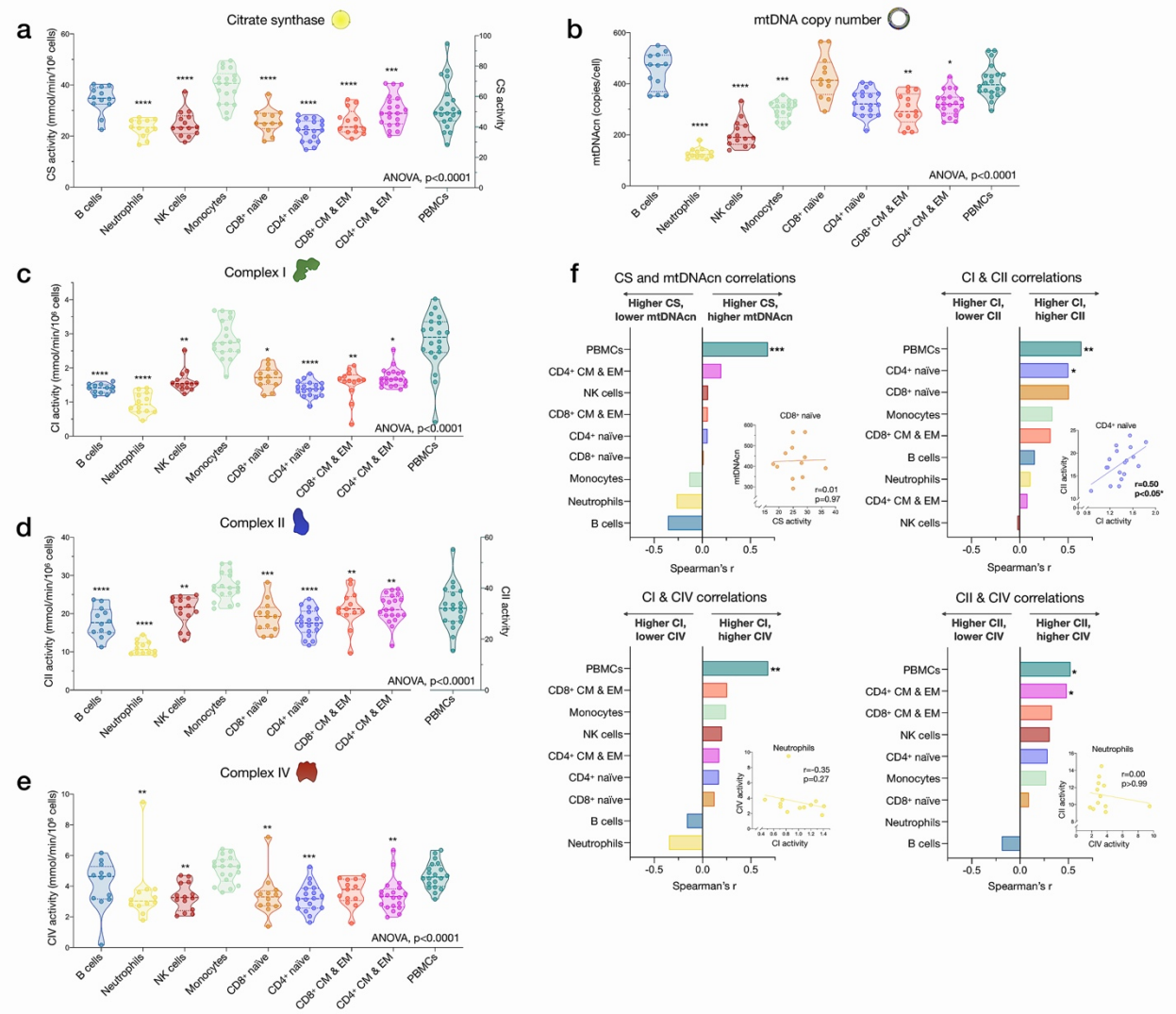

Figure 4 – Cell subtype differences in mitochondrial content and RC function. (**a-e**) Violin plots illustrating immune cell type differences in mitochondrial features across cell subtypes and total PBMCs. For each individual, only the 6 most abundant cell types were analyzed (n=21 individuals, 12-18 per cell subtype). Dashed lines are median (thick) and 25th and 75th quartiles (thin). P-values from One-Way non-parametric ANOVA Kruskal-Wallis test, post-hoc Dunn's multiple comparisons relative to PBMCs. (**f**) Spearman's r inter-correlations of mitochondrial features across subtypes. Insets show the scatterplots for selected correlations. p<0.05*, p<0.01**, p<0.001***, p<0.0001****.

Mitochondrial health index (MHI) among cell subtypes

We used the MHI composite to further define how RC function relates to mitochondrial content (Figure 5a). MHI significantly differed between cell types (p<0.0001). Monocytes had the highest MHI, which was 72% higher than B cells (g=3.78, p<0.0001), which had the lowest MHI (Figure 5b). On average, memory T cell subtypes exhibited a 6-18% higher MHI relative to their

naïve precursors (CD4$^+$: g=0.40, p=0.32; CD8$^+$: g=1.02, p=0.019), consistent with the notion that naïve and activated immune cells have different bioenergetic requirements[44, 45].

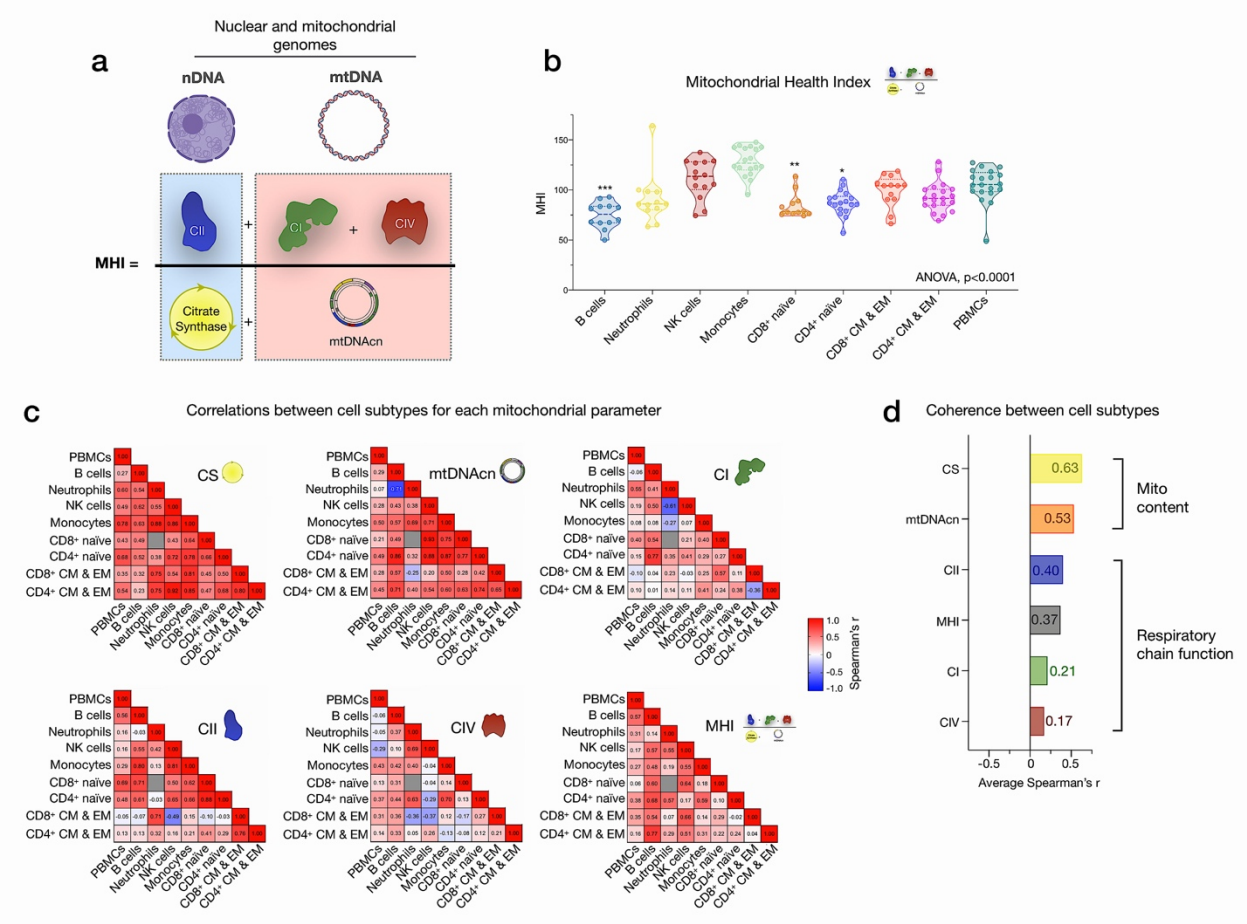

Figure 5 – Mitochondrial health index (MHI) and coherence of mitochondrial features across cell subtypes. (**a**) Schematic of the MHI equation reflecting respiratory chain function as the numerator, and markers of mitochondrial content as the denominator, yielding a metric of energy production capacity on a per-mitochondrion basis. (**b**) MHI across immune cell subtypes. Dashed lines are median (thick), with 25th and 75th quartiles (thin). P-values from One-Way non-parametric ANOVA Kruskal-Wallis test with Dunn's multiple comparison test of subtypes relative to PBMCs, n=12-18 per cell subtype. (**c**) Correlation matrices (Spearman's r) showing the association between cell subtypes in mitochondrial features. Correlations were not computed for cell subtype pairs with fewer than n=6 observations (gray cell). (**d**) Average effect sizes reflecting the within-person coherence of mitochondrial features across cell types (calculated using Fisher z-transformation). p<0.05*, p<0.001***.

Mitochondrial features exhibit differential co-regulation across immune cell subtypes

Next, we asked to what extent mitochondrial markers correlate across cell subtypes in the same person (co-regulation). For example, does the individual with the highest mtDNAcn in B

cells also have the highest mtDNAcn in all cell types? Could having high mtDNAcn or low MHI activity constitute coherent properties of an individual that are expressed ubiquitously across cell types, or are these properties specific to each cell subtype?

CS activity and mtDNAcn were moderately co-regulated across cell subtypes (average correlation $r_{z'}$=0.63 and 0.53, respectively) (Figure 5c-d). In comparison, RC enzymes showed markedly lower inter-correlations across cell types and some cell types showed no correlation with other cell types, revealing a substantially lower degree of co-regulation among RC components than in mitochondrial content features. MHI showed moderate and consistent positive co-regulation across cell types (average $r_{z'}$=0.37). Notably, PBMCs exhibited moderate to no correlation with other cell subtypes, further indicating their departure from purified subtypes. Together, these subtype-resolution results therefore provide a strong rationale for performing cell-type specific studies when examining the influence of external exposures and person-level factors on immune cells' mitochondrial bioenergetics, including the influence of sex and age.

Mitochondrial content and RC function differ between women and men

To evaluate the added value of cell subtype specific studies when applied to real-world questions, we systematically compared CS activity, mtDNAcn, RC activity, and MHI between women and men (Figure 6a-f). Across all cell subtypes examined, women had consistently higher CS activity (range: 4-29%, g=0.20-1.52, Figure 6a) and higher CII activity (range:1-10%, g=0.03-0.56, Figure 6d) than men. Women also had 26% higher CI activity than men (g=1.35) in monocytes (Figure 6c).

Compared to women, men exhibited higher mtDNAcn in monocytes and neutrophils (range: 5-12%, g=0.37-0.73, Figure 6b), higher CI activity in neutrophils and NK cells (range: 9-13%, g=0.26-0.64, Figure 4c), and higher CIV activity specifically in B cells (20%, g=0.53, Figure 6e). Cells exhibiting the largest degree of sexual dimorphism on the integrated MHI were neutrophils (17% higher in women, g=0.52) and B cells (12% higher in men, g=0.73) (Figure 6f). In contrast, none of these differences were detectable in PBMCs, illustrating the limitation of mixed cells to examine sex differences in mitochondrial function.

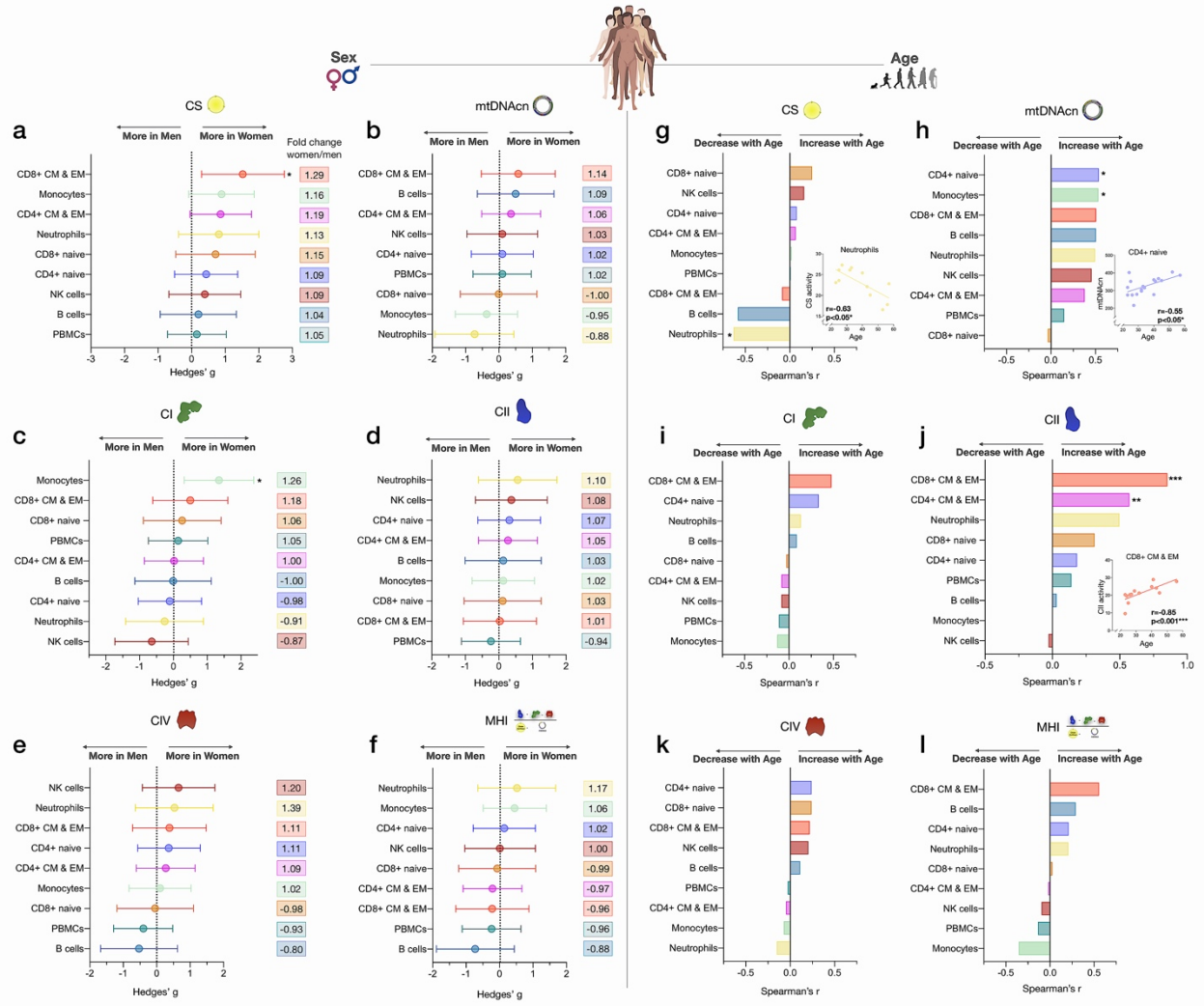

Figure 6 – Associations of mitochondrial features with sex and age across cell subtypes. (**a-f**) Effect size of sex differences in mitochondrial activity across cell subtypes quantified by Hedges' g. The fold change computed from raw values is shown on the right. P-values from Mann-Whitney test. Error bars reflect the 95% C.I. on the effect size. (**g-l**) Association of age and mitochondrial features across cell subtypes. P-values from Spearman's r correlations, not adjusted for multiple comparisons. n=21 (11 women, 10 men), p<0.05*, p<0.01**, p<0.001***.

Age associations with mitochondrial content and RC function

We then explored the association between mitochondrial features and age. With increasing age, CS activity was relatively unaffected except in neutrophils, where it decreased ~7% per decade (r=-0.63, p=0.031) (Figure 6g). In comparison, mtDNAcn increased with increasing age among all cell subtypes except $CD8^+$ naïve T cells, which is the cell type that exhibited the strongest age-related decline in abundance. $CD4^+$ naïve T cells and monocytes showed the largest age-related change in mtDNAcn, marked by a ~10% increase in the number of mitochondrial

genome copies per cell per decade of life (r=0.54 for both, p=0.022 and 0.023 respectively, Figure 6h).

For RC function, an equal number of cell subtypes with either positive or negative correlations with age were found, with the exception of CII (Figure 6i-l). CII activity was positively correlated with age across all cell types, except for monocytes and NK cells. In contrast, CI and CIV activities were only weakly associated with age, highlighting again differential regulation and partial "biological independence" of different RC components. Of all cell types, $CD8^+$ CM-EM T cells showed the most consistent positive associations for all RC activities and age, most notably for CII where the enzymatic activity per cell increased a striking ~21% per decade (r=0.85, p=0.0004).

Overall, these data demonstrate that age-related changes in CS activity, mtDNAcn, and RC function are largely cell-type specific. This conclusion is further reinforced by analyses of PBMCs where mitochondrial features consistently did not significantly correlate with age (r=0.008-0.15, absolute values) (Figure 6g-l).

Cell subtype distributions exhibit natural week-to-week variation

Samples collected weekly over 9 weeks from one repeat participant were used to examine whether and how much mitochondrial content/function change over time (Figure 7a). First focusing on immune cell distribution, the cell subtype with the least week-to-week variation in abundance was $CD8^+$ EM (root mean square of successive differences [rMSSD]=0.22, coefficient of variation [C.V.]=19.5%), which varied between 6.3% (week 2, highest) and 3.3% of all circulating cells (week 9, lowest) (Supplemental Figure 5). Other subtypes such as $CD4^+$ TEMRA (min=0.02% to max=0.62%) and neutrophils (min=3.9% to max=31.8%) varied week-to-week by an order of magnitude (i.e., 10-fold), similar to the between-person variation among the cohort (see Figure 1e and Supplemental Table 2). The circulating abundance of B cells varied by up to 1.1-fold (min=0.86% to max=1.8%). Together, these time-course results illustrate the dynamic remodeling of circulating leukocyte populations (and therefore PBMC composition) within a single person.

The correlations between immune cell type composition at each week and PBMCs mitochondrial features are shown in Supplemental Figure 6. On weeks when the participant had higher circulating levels of EM and TEMRA $CD4^+$ and $CD8^+$ lymphocytes, most mitochondrial features were considerably lower in PBMCs. The associations between CBC-derived cell proportions and PBMCs mitochondrial features tended to be weaker and in opposite direction at the within-person level compared to the cohort (Supplemental Figure 6c-d), but again document the influence of cell type composition on PBMCs mitochondrial phenotypes.

Mitochondrial content, mtDNAcn and RC activity exhibit natural week-to-week variation

The 6 most abundant cell subtypes analyzed for this individual included: neutrophils, NK cells, monocytes, naïve and CM-EM subtypes of $CD4^+$ T cells, and naïve $CD8^+$ T cells. The robust cell type differences in mitochondrial content and RC activities reported above in our cohort were conserved in the repeat participant. This includes high mtDNAcn in $CD8^+$ naïve T cells (average across 9 weeks=400 copies/cell, 427 in the cohort) and lowest mtDNAcn in neutrophils (average=123 copies/cell, 128 in the cohort).

All mitochondrial metrics exhibited substantial weekly variation across the 9 time points. Different cell types showed week-to-week variation in CS, mtDNAcn, and RC activity ranging from 4.1 to 64.4% (Figure 7b-f). MHI in each subtype varied by 8.3 to 20.6%, with the naïve subsets of $CD4^+$ and $CD8^+$ T lymphocytes exhibiting the largest week-to-week changes (rMSSD=0.28 and 0.22, respectively) (Figure 7g). In most cases, the observed variation was significantly greater than the established technical variation in our assays (see Supplemental Table 3), providing confidence that these changes in mitochondrial content and function over time reflect real biological changes rather than technical variability.

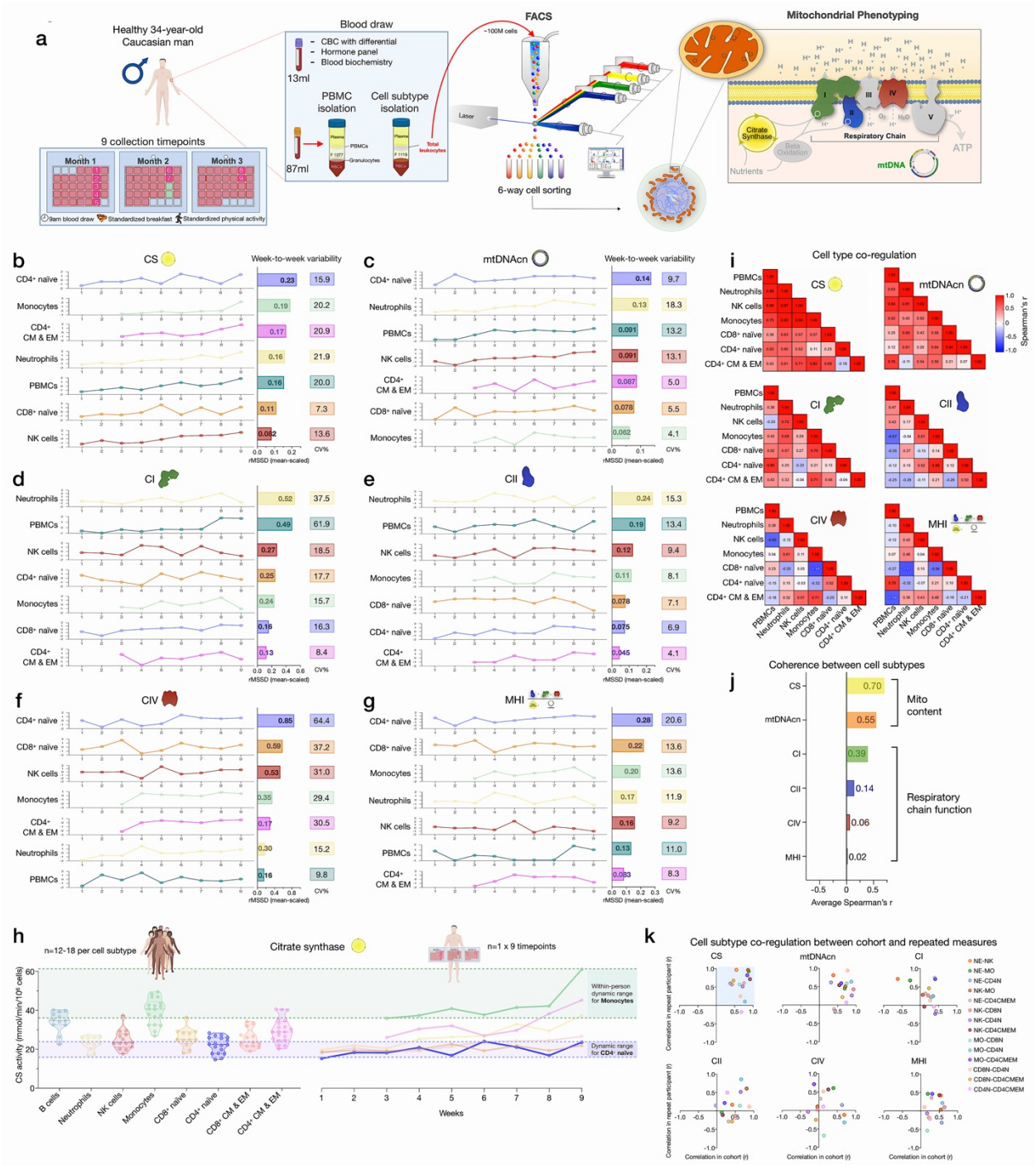

Figure 7 – Within-person variability of mitochondrial features across cell subtypes. (**a**) Overview of the repeat participant design, including blood collection, processing, and analysis. All samples were collected, stored, and processed as a single batch with samples from the cohort. Mitochondrial phenotyping platform schematic adapted from[10]. (**b-g**) Natural weekly variation for each mitochondrial feature across cell subtypes in the same person across 9 weeks represented as scaled centered data where 1 unit change represents a one-standard deviation (S.D.) difference. Root mean square of the successive differences (rMSSDs) quantify the magnitude of variability between successive weeks. The coefficients of variation (C.V.) quantify the magnitude of variability across all time points. Monocytes and CD4^{+} CM-EM were not

collected on weeks 1 and 2. (**h**) Side-by-side comparison of CS activity between the cohort (n=12-18 per cell subtype) and the repeat participant (n=7-9 time points) across cell subtypes. The dynamic range of two cell subtypes are highlighted: monocytes and $CD4^+$ naïve T cells. (**i**) Within-person correlation matrices between cell subtypes for each mitochondrial feature over 9 weeks, illustrating the magnitude of correlation (co-regulation) between cell subtypes. (**j**) Average inter-correlation across all cell subtypes by mitochondrial feature (calculated using Fisher z-transformation) indicating the degree of coherence within-person. (**k**) Comparison of co-regulation patterns among mitochondrial features between the cohort and the repeat participant. Each datapoint represents a cell subtype pair, indicating moderate agreement (datapoints in top right quadrant).

We then asked how much the same metrics naturally vary within a person relative to differences observed between people in the heterogeneous cohort. Remarkably, the 9-week range of natural variation within the same person was similar to the between-person differences among the cohort. Figure 7h and Supplemental Figure 7 provide a side-by-side comparison of the cohort and repeat participant mitochondrial features (CS, mtDNAcn, RC activities, and MHI) on the same scale. A similar degree of variation (9.8-61.9%) was observed in PBMCs (Figure 7b-g), although again this variation may be driven in large part by variation in cell composition.

And as in the cohort, CS and mtDNAcn were also most highly correlated across cell types (average $r_{z'}$=0.55-0.70) (Figure 7i-k, Supplemental Figure 6e), indicating partial co-regulation of mitochondrial content features across cell subtypes.

Mitotypes differ between immune cell subtypes

To examine cell type differences more fully and in line with the concept of mitochondrial functional specialization, we performed exploratory analyses of cell subtype-specific mitochondrial phenotypes, or *mitotypes*, by mathematically combining multiple mitochondrial features in simple graphical representation (listed and defined in Supplemental Figure 8). Each mitotype can be visualized as a scatterplot with two variables of interest as the x and y axes (Figure 8a).

The first mitotype examined puts in relation mtDNA copies per cell (mtDNAcn) relative to mitochondrial content per cell (CS activity), creating a mitotype (mtDNAcn/CS) reflecting *mtDNA density per mitochondrion* (Figure 8b). Alone, the mtDNA density per mitochondrion mitotype provided remarkable separation of cell subtypes. Neutrophils and NK cells were low on both metrics, B cells were high on both metrics, monocytes had the lowest mtDNA density,

whereas $CD8^+$ naïve T cells exhibited the highest mtDNA density of all cell subtypes tested. Figure 8c-e illustrate other mitotypes including i) CII activity per unit of mitochondrial genome (CII/mtDNAcn), as well as more complex combinations of variables such as ii) CI activity per mtDNA (CI/mtDNAcn ratio on y axis) in relation to mtDNA density (mtDNAcn/CS activity on x axis), and iii) CI activity per mitochondrial content (CI/CS, y axis) in relation to mtDNA density (mtDNAcn/CS, x axis). As Figure 8b-e shows, PBMCs generally exhibit a similar mitotype (diagonal line from the origin of the plot) as innate immune cell subtypes (monocytes, NK cells, and neutrophils), and are relatively distinct from lymphocyte subpopulations.

This mitotype-based analysis revealed two main points. First, cells of the innate and adaptive immune subdivisions contain mitochondria that differ not only quantitatively in their individual metrics of mitochondrial content and RC activity, but also qualitatively, as illustrated by the distinct clustering of neutrophils, monocytes and NK cells (innate) within similar mitotype spaces and the clustering of all lymphocyte subtypes together in a different space. Compared to cells of the innate immune compartment, lymphocytes (adaptive) had higher mtDNAcn and lower respiratory chain activity. Second, compared to naïve subsets of $CD4^+$ and $CD8^+$ T cells, which themselves have relatively distinct mitotypes (e.g., CII/mtDNAcn, Figure 8c), both memory $CD4^+$ and $CD8^+$ subtypes converged to similar mitotype spaces. Functionally, this naïve-to-memory transition is well known to involve a metabolic shift including changes in spare respiratory capacity, mitochondrial content, glucose and fatty acid uptake[44, 46]. The mitotype analysis showed that compared to naïve cell subtypes, memory subtypes exhibit 26-29% lower mtDNA density per mitochondrion, but an 8-23% increase in RC activity per mitochondrion in $CD4^+$ T cells, although not in $CD8^+$ T cells (Figure 8f).

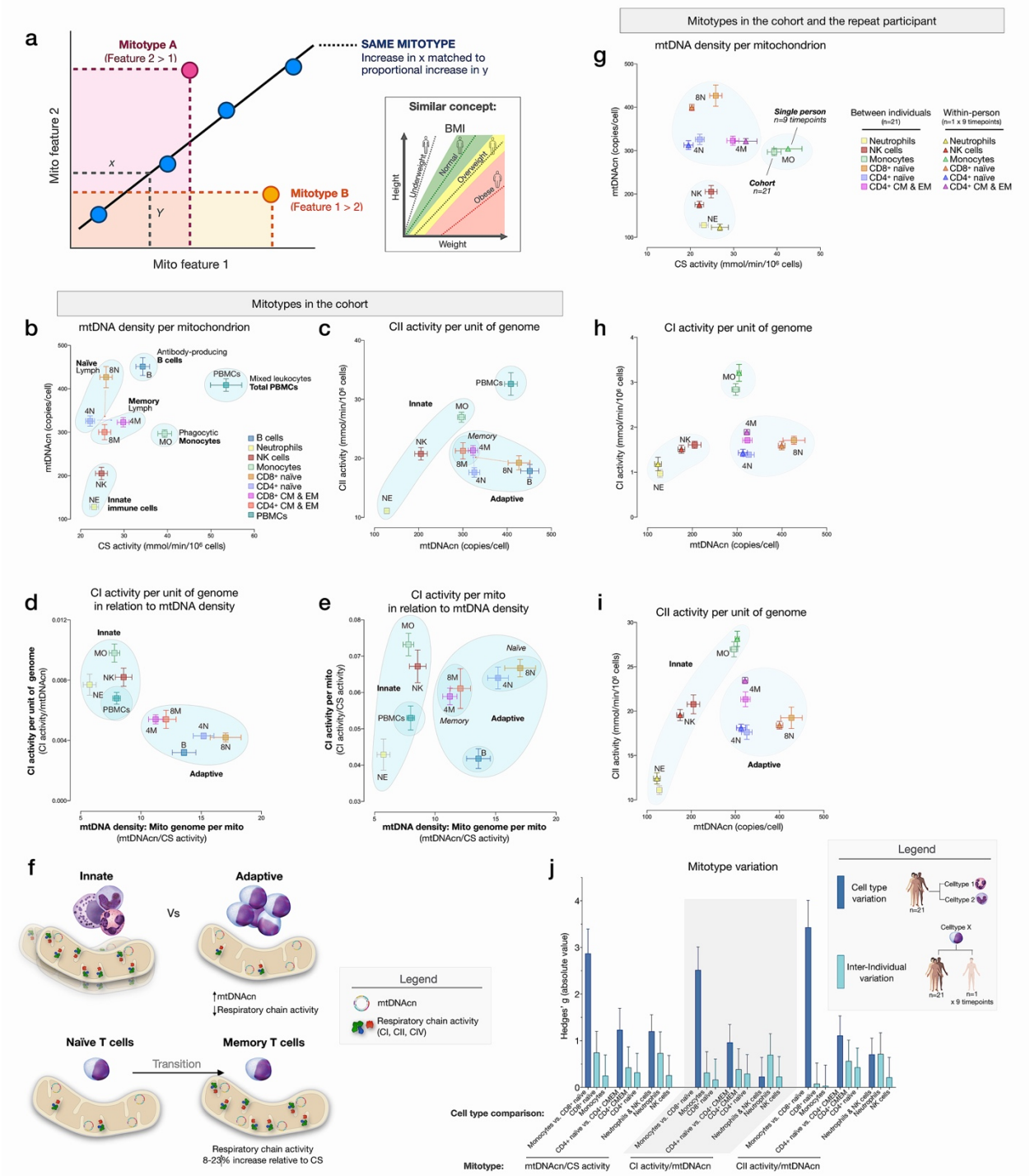

Figure 8 – Mitotypes in purified leukocyte populations from the cohort and repeated-measures. (**a**) Schematic illustrating the multivariate approach to generate and visualize mitotypes by putting into relation two or more mitochondrial features. Note the similarity and added insight relative to single metrics, similar to the integration of height and weight into the body mass index (BMI). (**b-e**) Selected mitotypes plotted for each cell subtype among the cohort. Data are means ± SEM (n=12-18). Overlaid shaded areas denote general leukocyte categories, for visualization purposes only. (**f**) Summary of mitotype differences between (i) innate vs adaptive subdivisions, and (ii) naïve vs memory T cells. (**g-i**) Validation of subtype-specific

mitotype differences in the repeat participant, illustrating the conserved nature of mitotypes across individuals. Only the six cell subtypes analyzed in the repeat participant are plotted. Data are means ± SEM (n=7-9 for the repeat participant, 12-18 for the cohort). (**j**) Comparison of the magnitude of the difference (Hedges' g) in mitotypes between cell types, and between individuals. Dark blue bars indicate the magnitude of the dominant difference in mitotypes between cell subtypes. Light blue bars indicate the magnitude of the difference between the cohort and the repeat participant within a cell type. Error bars are the 95% C.I. of the effect size.

Stability of mitotypes

Plotting matching cell types for the cohort and the repeat participant on the same mitotype plots showed a high degree of agreement. Again, cell types belonging to the innate and adaptive immune subdivisions similarly clustered together, and naïve and memory subtype differences were similarly validated at the within-person level (Figure 8g-i), demonstrating the conserved nature of immune cell mitotypes in our sample. On average, the magnitude of variation between cell subtypes (e.g., monocytes vs neutrophils) was 12.5-fold larger than the differences between the cohort and the participant, indicating that immune cell subtypes have distinct mitotypes that are relatively stable across individuals.

Evidence for a sex and age bias in mitotypes

We next sought to systematically examine if mitotypes differ between women and men. Mitotypes were organized into five categories of indices based upon their features, yielding a total of 16 mathematically-distinct mitotypes (see Supplemental Figure 8). For each mitotype, we quantified the magnitude of the difference between women and men by the effect size (g), ranked all mitotype x cell subtype combinations (16 mitotypes x 9 cell subtypes), and analyzed the distribution of these indices by sex. The majority of mitotypes reflecting mitochondrial RC activities per CS activity were higher in men ($p<0.0001$, Chi-square), while RC activity per mtDNA density ($p<0.001$) and RC activity per genome in relation to mtDNA density mitotypes ($p<0.01$) were predominantly higher in women (Figure 9a). The magnitude of sex differences ranged from 17% higher in men (CI/CS in $CD4^+$ CM-EM T cells, g=1.14) to 38% higher in women (CII/mtDNA density in neutrophils, g=1.37) (Figure 9b). The direction of sex differences for all mitotypes (e.g. higher in women or in men) with effect sizes is illustrated in Figure 9c**.** The average effect size across all mitotypes was 0.31 (small) in $CD4^+$ naïve T cells, compared to monocytes where the average effect size was 0.71 (medium). Compared to purified cell subtypes, the magnitude of sex differences in PBMCs was blunted.

Using the same approach, we then systematically quantified the relationship between mitotypes and age. Mitotypes reflecting RC activity per CS activity were predominantly positively correlated with age (p=0.046), while RC activities per genome in relation to mtDNA density were generally negatively correlated with age (p=0.012) (Figure 9d). This finding is consistent with the overall age-related increase in mtDNAcn across cell subtypes, and could indicate a general decrease in the RC output per unit of mitochondrial genome with aging in immune cells. The strength of these correlations ranged from r=-0.67 to 0.75 (Figure 9e). The correlations of individual mitotypes with age for each cell subtype are shown in Figure 9f. Again, PBMCs showed among the weakest associations with either sex or age (Figure 9c and f). Thus, even if specific cell subtypes reveal consistent sex- and age-related differences, PBMCs offer modest to no sensitivity to detect these associations.

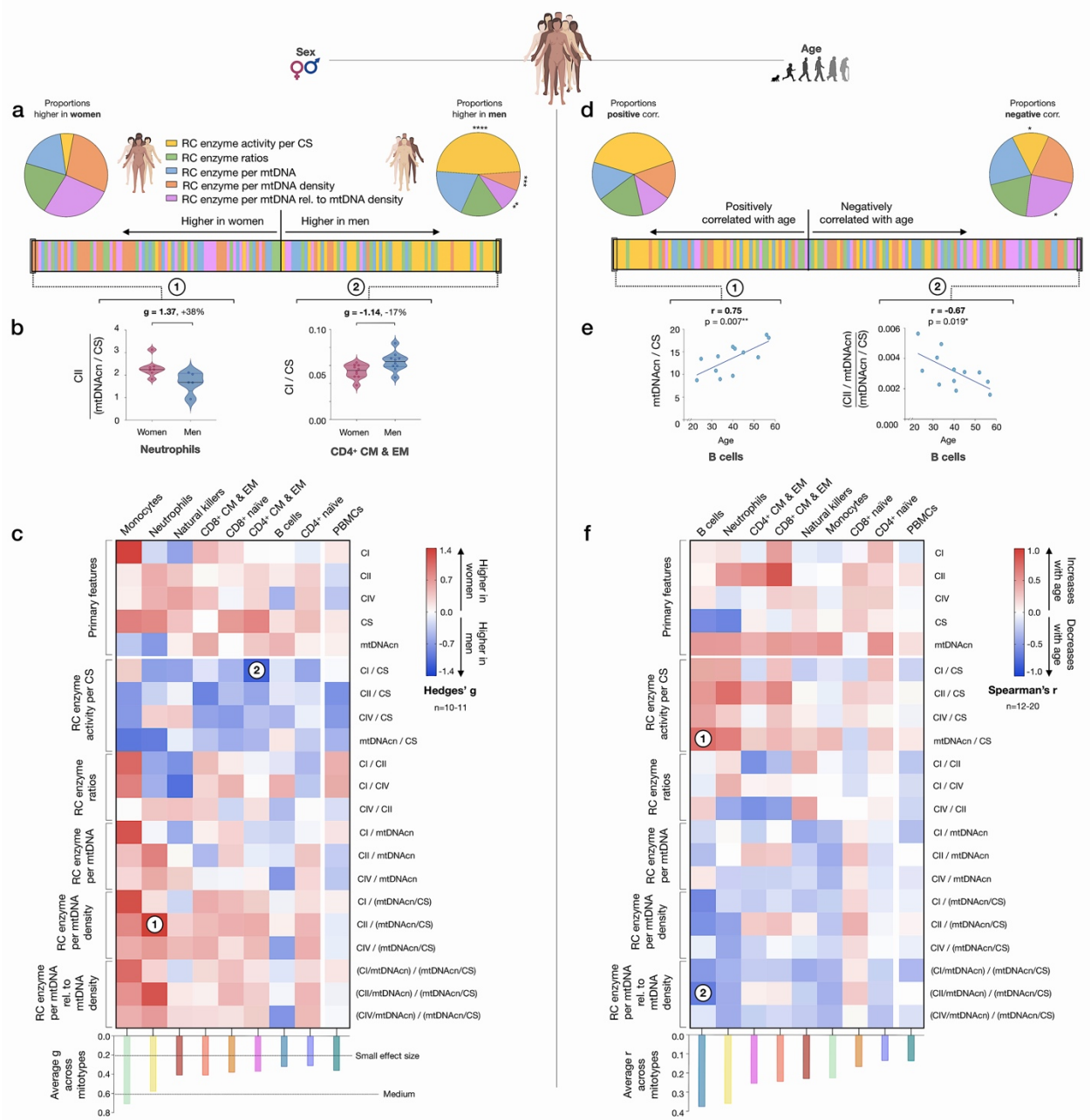

Figure 9 – Mitotype distribution and strength of difference across sex and age. (**a**) Ranking of mitotype indices by the effect size (Hedges' g) between women and men. A total of 16 mitotype indices were computed, subdivided into 5 main color-coded categories (see Supplemental Figure 8). Pie charts illustrate the proportion mitotypes belonging to each category that are either higher in women (*left*) or in men (*right*). P-values for enrichment of sexually dimorphic mitotypes are derived from Chi-square test. (**b**) Violin plots illustrating the two mitotypes with the largest sex differences, both showing large effect sizes (g). (**c**) Heatmap of sex differences for primary measures of mitochondrial function (*top*) and multivariate mitotypes (*bottom*) across cell subtypes. The histogram at the bottom shows the average effect size across all mitotypes (calculated from absolute g values). (**d**) Ranking of mitotype indices by the strength and direction of their association with age, with enrichment analysis analyzed as for sex (Chi-square test). (**e**)

Spearman's r correlations of mitotypes/cell type combinations with the strongest positive and negative associations with age. (**f**) Heatmap of the age correlations (Spearman's r) for primary features and composite mitotypes across cell subtypes. The histogram (*bottom*) shows the average effect size (r) for each cell subtype (calculated using absolute values and Fisher z-transformation). $p<0.05$*, $p<0.01$**, $p<0.001$***, $p<0.0001$****.

Associations of blood biomarkers with subtype-specific mitochondrial features

To explore the source of inter-individual differences and within-person dynamics over time described above, we asked to what extent subtype-specific mitochondrial features were correlated with blood biomarkers, including a panel of sex hormones, inflammatory markers, metabolic markers, and standard clinical blood biochemistry (Figure 10a).

At the cohort level, sex- and age-adjusted partial correlations between blood biomarkers and cell subtype mitochondrial phenotypes were relatively weak (average absolute values $r_{z'}=0.23$, Figure 10b), indicating that circulating neuroendocrine, metabolic and inflammatory factors are unlikely to explain a large fraction of the variance in inter-individual differences in mitochondrial biology. At the within-person level, week-to-week variation is independent of constitutional and genetic influences, and behavior (e.g., levels of physical activity, sleep patterns, etc.) is more stable relative to women and men of different ages. Compared to the cohort, the strength of biomarker-mitochondria associations was on average 70% larger in the repeat participant ($r_{z'}=0.39$) (Figure 10c). In particular, lipid levels including triglycerides, total cholesterol, and low- and high-density lipoproteins (LDL, HDL) were consistently positively correlated with markers of mitochondrial content (CS activity and mtDNAcn), with the largest effect sizes observed among innate immune cells: neutrophils, NK cells, and monocytes (Figure 10c, red area on the heatmap). In these cells, lipid levels accounted on average for 53% of the variance (r^2) in CS activity and 47% in mtDNAcn, possibly reflecting an effect of lipid signaling on mitochondrial biogenesis[47-50]. We also note divergences in the correlation patterns between the cohort and repeat participant (Figure 10d-e), possibly highlighting the potential value of repeated-measures designs to examine the influence of metabolic and other humoral factors on immune mitochondrial biology.

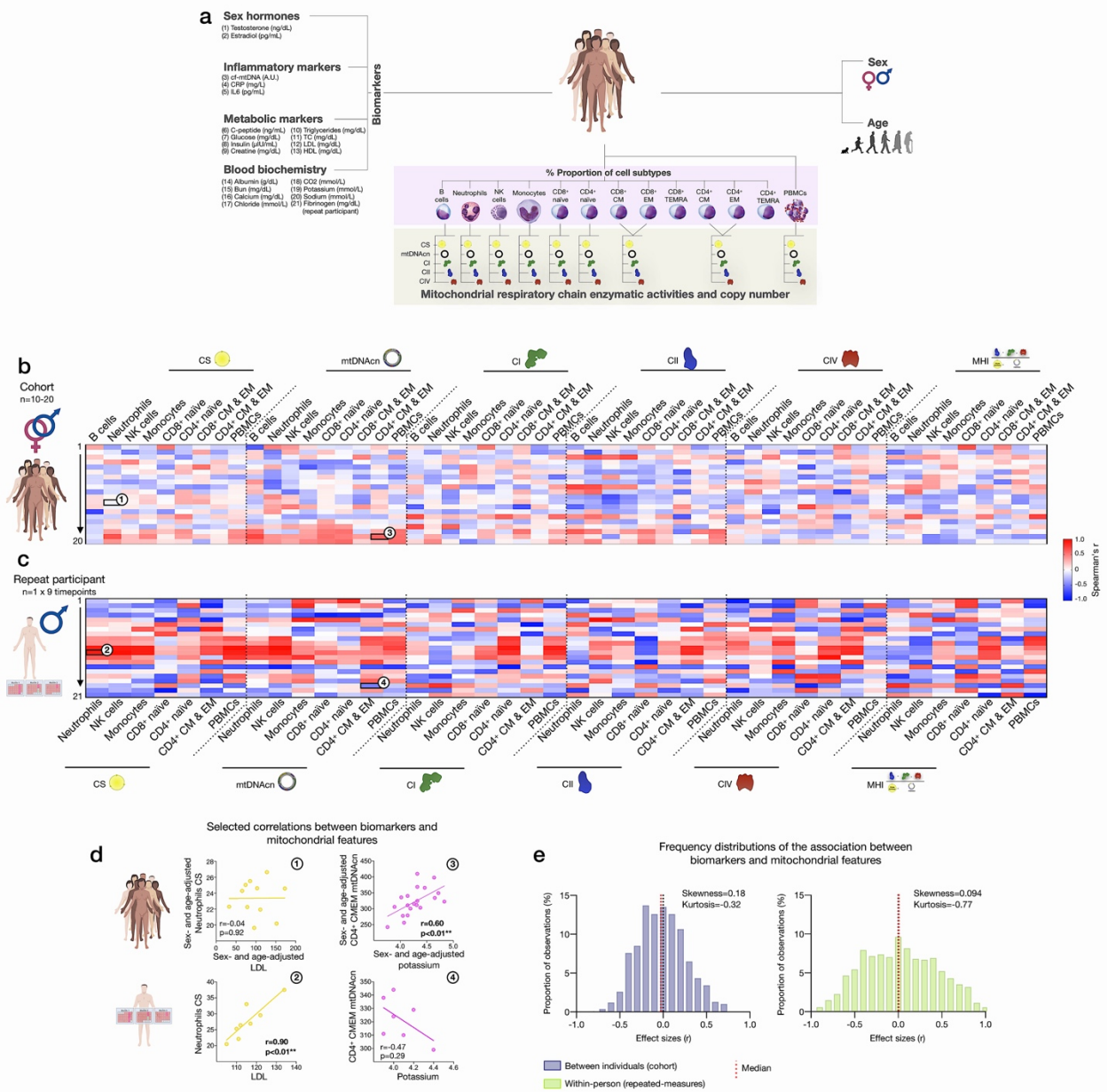

Figure 10 – Association of blood biomarkers with mitochondrial parameters across cell subtypes and primary mitochondrial features. (**a**) Overview of blood biochemistry, hormonal, and metabolic biomarkers collected for each participant. (**b**) Sex- and age-adjusted correlations between blood biomarkers and mitochondrial features across cell subtypes for the cohort (n=10-20 per mito:biomarker combinations) shown as a heatmap. (**c**) Same as (b) using weekly measures of both mitochondrial features and biomarkers in the repeat participant. (**d**) Scatterplots of the indicated correlations between Neutrophils CS activity and LDL cholesterol (*left*), and $CD4^+$ CM-EM mtDNAcn and potassium (K^+) (*right*) for the cohort (*top row*) and the repeat participant (*bottom row*). (**e**) Frequency distributions of the aggregated effect sizes between biomarkers and mitochondrial features across cell subtypes for the cohort (total correlation pairs=1,080) and the repeat participant (total correlation pairs=882).

Discussion

Developing approaches to quantify bioenergetic differences among various tissues and cell types is critical to define the role of mitochondria in human health and disease. Here we isolated and phenotyped multiple immune cell subtypes and mixed PBMCs in a diverse cohort of women and men, and in repeated weekly measures in the same participant. A high-throughput mitochondrial phenotyping platform in >200 person-cell type combinations defined large-scale functional differences in mitochondrial content and RC function between immune cell subtypes. We also found evidence that mitochondrial phenotypes vary with age and sex, which PBMCs did not have the sensitivity to detect. Our results show that PBMCs mitochondrial measurements are confounded by i) cell type composition, ii) platelet contamination, iii) mitochondrial properties across different cell subtypes, and iv) the dynamic remodeling of cell type composition and bioenergetics over time. In addition, large week-to-week, within-person variation in both cell subtype proportions and mitochondrial behavior pointed to heretofore underappreciated dynamic regulation of mitochondrial content and function over time. Finally, multivariate mitotypes provided a first step towards identifying stable cell-type specific bioenergetic profiles for future research. Together, these data in immunologically-defined leukocyte populations among a small cohort of healthy adults provide foundational knowledge of mitochondrial phenotypes in circulating human immune cells, and highlight the value of repeated-measures designs to examine the mechanisms of dynamic mitochondrial variation in humans.

This study highlights the value of using purified cell populations over PBMCs for mitochondrial analyses. In many cases, associations with moderate to large effect sizes in specific cell subtypes were either not observed or blunted in PBMCs. For example, there was no correlation between age and PBMCs MHI either in this study or previously[51], but there was in purified cell subtypes. Total PBMCs and cells of the innate subdivision, namely neutrophils, NK cells, and monocytes, had similar mitotypes (along the same mitotype diagonal space on mitotype plots). In the mitotype plots, if PBMCs were composed uniquely of a mixture of lymphocytes and monocytes, the natural expectation is that PBMCs would lie somewhere between the specific subsets that compose it. Instead, PBMCs occupy an entirely different and unexpected mitotype space. Our platelet depletion experiment leaves little doubt that platelet contamination skews the

measurements of several mitochondrial features in PBMCs, with some features being apparently more affected than others, and yielding contradictory results: for example, PBMCs have higher CS activity values than any of the constituent cells (see Figure 4a). Although we cannot entirely rule out potential contamination of individual cell types with residual platelets, the FACS labeling, washing, and sorting procedures produce the purest sample with the highest degree of biological specificity.

A major frontier for the human immunometabolism field consists in defining temporal trajectories of change over time in specific cell types[52]. Achieving this goal promises to transform knowledge of immune and mitochondrial biology and allow for rational design of therapeutic approaches for immunometabolic conditions[52]. A primary finding from our analyses is the natural within-person variation in mitochondrial features, providing initial insight into the temporal dynamics of immunometabolism in specific human cell subtype populations. Sorting immunologically-defined cell subtypes removed the potential confound of week-to-week changes in cell type distributions, an inherent confounding variable in PBMCs, and therefore adds confidence in the robustness of the reported temporal mitochondrial variation. Mitochondrial features within immune cells exhibited state-like properties that varied by >20-30% week-to-week, warranting future study of causal influences. Previously, in PBMCs, up to 12% of the inter-individual variation in MHI was attributable to positive mood (e.g., excited, hopeful, inspired, love) the night prior to blood draw[10], implying that psychosocial factors could in part contribute to dynamic variation in leukocyte mitochondrial function over 24 hours. However, limitations in this prior study – including the use of PBMCs and a single measurement time point for MHI – call for additional work to disentangle the independent contributions of behavioral, psychosocial, nutritional, and other factors on mitochondrial features in humans. Importantly, here mitochondrial changes took place within less than one week. Therefore, establishing the exact temporal dynamics of leukocyte mitochondrial variations and immunometabolism in general will require repeated assessments with even higher temporal resolution. As for other biological markers with high intra-individual variability (e.g., cortisol[53]), repeated-measures designs are required to reliably capture stable inter-individual differences.

Animal studies have consistently identified sexually dimorphic mitochondrial features, including greater mitochondrial content in females (reviewed in [54]). Likewise, in humans, PBMCs

from women had greater CS activity and greater CI and CII-mediated respiration[55]. Our data show similar changes in enzymatic activities for most, but not all, cell types, suggesting that the magnitude of sex differences is likely cell-type specific. Therefore, methods offering a sufficient level of biological specificity could reproducibly and accurately quantify sex differences in different contexts.

Age-related decline in mtDNAcn has been observed in whole blood[41, 42], PBMCs[43], and skeletal muscle tissue[56, 57], but not liver[58]. However, cell mixtures and platelet contamination must be considered, particularly for blood and PMBCs[22, 23]. Accounting for cell type distribution and platelet count through measurement and statistical adjustments eliminated initial associations between mtDNAcn and age in a large adult sample[59]. mtDNA mutations and deletions accumulate with age (e.g.,[43, 60]), and mtDNA defects can trigger the compensatory upregulation of mtDNAcn to counteract the loss of intact mitochondria associated with age[61, 62]. Therefore, the observed positive correlation of cell type-specific mtDNAcn with age in our sample could reflect compensatory upregulation of mtDNA replication. Alternatively, this correlation could reflect impaired autophagic removal in aging cells, consistent with recent results in $CD4^+$ T cells[34]. The only cell type examined that did not exhibit positive correlation between mtDNAcn and age was $CD8^+$ naïve T cells, which is also the only cell type whose abundance in circulation significantly declines with advancing age. The basis for the direction of this association requires further investigation.

Some limitations of this study must be noted. Although this represents, to our knowledge, the largest available study of mitochondrial biochemistry and qPCR in hundreds of samples, the sample size of the cohort and power to examine between-person associations was small. Women and men were equally represented, but the sample size precluded stratification of all analyses by sex. Likewise, the exhaustive repeated-measures design was carried out in only one participant and should be regarded as proof-of-concept. Additionally, because our mitochondrial phenotyping platform currently requires ~$5x10^6$ cells per sample, we could only collect the six most abundant cell subtypes from each participant, which in some instances reduced the final sample size for different cell subtypes. In order to accommodate the minimum cell number per sample, central and effector memory subtypes were pooled (CM-EM), although they may exhibit differences not examined here. Furthermore, we recognize that additional cell surface markers may be useful to

identify other cell populations (e.g., activated or adaptive lymphocyte subtypes). Finally, we did not test participants for CMV status, which could contribute to proportion of immune cell subtypes.

Our analysis focused on RC activity, which performs electron transport and generates the mitochondrial membrane potential ($\Delta\Psi m$) across the inner mitochondrial membrane[63]. Besides being used for ATP synthesis by Complex V, RC activity and membrane potential also contributes to reactive oxygen species (ROS) production, calcium handling, and regulates gene expression[64-67]. Thus, similar to observations in animal models[68], the observed cell type differences in mitochondrial content or RC activities across human immune cell subtypes could reflect not only cellular ATP demand, but also other unique immunometabolic, catabolic/anabolic, and signaling requirements among different immune cell subtypes.

Overall, mitochondrial profiling in circulating human immune cells filled three main knowledge gaps. Mitochondrial profiling defined confounds for PBMCs and showed how PBMCs fail to capture age- and sex-related mitochondrial recalibrations in specific immune cell populations, which is important for the design of future studies. Second, mitochondrial profiling precisely documented large-scale, quantitative differences in CS activity, mtDNAcn, and RC enzyme activities between well-known immune cell subtypes, representing foundational knowledge of the metabolic characteristics in key circulating immune cell types in humans. Our mitotype approach also identified conserved multivariate phenotypic distinctions between lymphoid- and myeloid-derived immune cells, and naïve-to-memory lymphocyte states. Third, this study documents potentially large week-to-week variation of mitochondrial activities that should be further examined in future studies. Together, this work provides foundational knowledge to develop interpretable blood-based assays of mitochondrial health.

Methods

Participants and Procedures

A detailed account of all methods and procedures is available in the *Supplementary document*. The study was approved by New York State Psychiatric Institute (Protocol #7618) and all participants provided written informed consent for the study procedures and reporting of results. Healthy adults between 20 and 60 years were eligible for inclusion. Exclusion criteria included severe cognitive deficit, symptoms of flu or other seasonal infection four weeks preceding the visit, involvement in other clinical trials, malignancy or other clinical condition, and diagnosis of mitochondrial disease. The main study cohort included 21 individuals (11 women, 10 men), with mean age of 36 years (SD= 11, range: 23-57); there were 2 African Americans, 7 Asians, and 12 Caucasians. Morning blood samples (100 ml) were drawn between 9-10am from the antecubital vein and included one EDTA tube for complete blood count (CBC), two SST coated tubes for hormonal measures and blood biochemistry, and 11 Acid Dextrose A (ACD-A) tubes for leukocyte isolation and mitochondrial analyses. See Figure 1a-b for an overview of participants and procedures.

Additionally, repeated weekly measures were collected across 9 weeks from one healthy Caucasian man (author M.P., 34 years old) to assess within-person variability in mitochondrial measures and immune cell type distribution. To standardize and minimize the influence of nutritional and behavioral factors in the repeat participant, repeated measures were collected at the same time (9:00am), on the same day of the week (Fridays), after a standardized breakfast (chocolate crepe), ~30-60 minutes after a regular bicycle commute to study site.

PBMCs and leukocyte isolation

A detailed version of the materials and methods is available in the online Supplement of this article. Briefly, PBMCs were isolated on low density Ficoll 1077, and total leukocytes were separated on Ficoll 1119, centrifuged at 700 x g for 30 minutes at room temperature. Leukocytes were collected, washed, and centrifuged twice at 700 x g for 10 minutes to reduce platelet contamination. Pellets of $5x10^6$ PBMCs were aliquoted and frozen at -80ºC for mitochondrial assays.

Immunolabeling and fluorescence-activated cell sorting (FACS)

Antibody cocktails for cell counting (Cocktail 1) and cell sorting (Cocktail 2) were prepared for fluorescence-activated cell sorting (FACS). The following cell subtypes were identified: neutrophils, B cells, monocytes, NK cells, naïve $CD4^+$ and $CD8^+$, central memory (CM) $CD4^+$ and $CD8^+$, effector memory (EM) $CD4^+$ and $CD8^+$, and terminally differentiated effector memory cells re-expressing CD45RA (TEMRA) $CD4^+$ and $CD8^+$ (see Supplemental Figure 1 and Table 1 for overview, and Supplemental Table 4 for cell surface markers and fluorophores). A $2x10^6$ cell aliquot was labeled with Cocktail 1. The remainder of total leukocytes (~$100x10^6$ cells) were incubated with Cocktail 2, washed, and used for FACS at final concentration of $20x10^6$ cells/ml.

Leukocytes were sorted using a BD™ Influx cell sorter using a 100 µm size nozzle. Sorting speed was kept around 11,000-12,000 events/second. Cell concentration for sorting was measured at about $15x10^6$ cells per ml. For each participant, $1x10^6$ cells (Cocktail 1 panel) were run first to calculate the potential yield of each subpopulation (total cell number x percentage of each subpopulation). The variable proportions of cell subtypes from person-to-person (provided in full in Supplemental Table 2) determined which cell subtypes were collected from each participant, and $5x10^6$ cell aliquots of the six most abundant subpopulations were sorted. Purity checks were performed on all sorted subpopulations to ensure the instrument performance was good enough to reach the sorted population purity >95%. Data were processed using FCS Express 7 software (see Supplemental Figure 2 for gating strategy).

Mitochondrial enzymatic activities

Sorted cell subtypes were centrifuged at 2,000 x g for 2 minutes at 4°C and stored in liquid nitrogen (-170°C) for 4-12 months until mitochondrial biochemistry and mtDNAcn analyses were performed as a single batch. Cell pellets ($5x10^6$) were mechanically homogenized with a tungsten bead in 500 ul of homogenization buffer as previously described[10] (see *Supplement* for details).

Mitochondrial enzyme activities were quantified spectrophotometrically for citrate synthase (CS), cytochrome c oxidase (COX, Complex IV), succinate dehydrogenase (SDH, Complex II), and NADH dehydrogenase (Complex I) as described previously[10] with minor modifications described in the Supplement. Each sample was measured in triplicates. Mitochondrial enzymatic activities were measured on a total of 340 samples (including 136

biological replicates), for a total of 204 unique participant-cell combinations. The technical variation for each enzyme, for each cell type, is detailed in Supplemental Table 3.

Mitochondrial DNA copy number

mtDNAcn was determined as described previously[10] using two different Taqman multiplex assays for ND1 (mtDNA) and B2M (nDNA), and for COX1 (mtDNA) and RnaseP (nDNA). mtDNAcn was calculated from the ΔCt obtained by subtracting the mtDNA Ct from nDNA Ct for each pair ND1/B2M and COX1/RNaseP, and mtDNAcn from both assays was averaged to obtain the final mtDNAcn value for each sample. The coefficients of variation (C.V.) for mtDNA for each cell subtype is detailed in Supplemental Table 3 (average 5.1%).

Platelet depletion in PBMCs

A further 9 community-dwelling older adults (mean age = 79, range: 64-89, 4 women and 5 men, including 7 White and 2 African American participants) were recruited for active platelet depletion experiments. Exclusion criteria included diseases or disorders affecting the immune system including autoimmune diseases, cancers, immunosuppressive disorders, or chronic, severe infections; chemotherapy or radiation treatment in the 5 years prior to enrollment; unwillingness to undergo venipuncture; immunomodulatory medications including opioids and steroids; or more than two of the following classes of medications: psychotropics, anti-hypertensives, hormones replacement, or thyroid supplements. Participants were recruited from a volunteer subject pool maintained by the University of Kentucky Sanders-Brown Center on Aging. The study was conducted with the approval of the University of Kentucky Institutional Review Board. Morning blood samples (20 mL) were collected by venipuncture into heparinized tubes. PBMCs were isolated from diluted blood by density gradient centrifugation (800 x g for 20 minutes) using Histopaque. Buffy coats were washed once, and cells were counted using a hemocytometer. PBMCs (20-30 M) were cryopreserved in liquid nitrogen in RPMI-1640 with 10% FBS and 10% DMSO until further processing.

For active platelet depletion, PBMCs were first thawed at room temperature and centrifuged at 500 x g for 10 minutes, counted and divided into 2 aliquots, including $10x10^6$ cells for total PBMCs, and $11x10^6$ cells for platelet depletion. The total PBMCs were centrifuged at 2,000 x g for 2 min at 4°C and frozen as a dry pellet at -80°C until processing for enzymatic assays and qPCR. The PBMCs destined for platelet depletion were processed immediately and depleted

of platelets following manufacturer procedures using magnetically-coupled antibodies against the platelet marker CD61. This experiment yielded three samples per participant, including total PBMCs, platelet depleted PBMCs, and enriched platelets. Each sample was processed in parallel for RC enzymatic activity assays and mtDNAcn as described above.

Statistical analyses

To adjust for potential order and batch effects across the 340 samples (31 samples per 96-well plate, 17 plates total), a linear adjustment was applied to raw enzymatic activity measures to ensure consistency between the first and last samples assayed. Samples from both the cohort and repeat participant were processed and analyzed as a single batch, ensuring directly comparable data.

Throughout, standardized effect sizes between cell subtypes and between groups were computed as Hedges' g (g). Mann-Whitney T tests were used to compare sex differences in cell type proportions and mitochondrial measures. Spearman's r (r) was used to assess strength of associations between continuous variables such as age and circulating proportions of cell subtypes. To assess to what extent mitochondrial features are correlated across cell subtypes (co-regulation) and to calculate the average correlation across mitotypes, Spearman's r matrixes were first computed and transformed to Fisher's Z', and then averaged before transforming back to Spearman's r ($r_{Z'}$). One-way non-parametric ANOVA Kruskal-Wallis with post-hoc Dunn's multiple comparison tests were used to compare cell type mitochondrial measures in different cell subtypes and PBMCs. Between- and within-person variation were characterized using coefficients of variation (C.V.). The root mean square of successive differences (rMSSD) was computed to quantify the magnitude of variability between successive weeks for repeated measures. Chi-square tests were computed to compare proportion of mitotype indices categories (enzyme activity per CS, enzyme ratios, enzyme per mtDNA, enzyme per mtDNA density, and enzyme per mtDNA relative to mtDNA density) by age (lower vs higher with increased age) and sex (lower vs higher in men). Finally, one-way non-parametric Friedman tests with post hoc Dunn's multiple comparisons were used to compare mitochondrial measures in platelet-depleted PBMCs, enriched platelets PBMCs, and total PBMCs. Statistical analyses were performed with Prism 8 (GraphPad, CA), R version 4.0.2 and RStudio version 1.3.1056. Statistical significance was set at $p<0.05$.

Data Availability

Upon acceptance, the authors will upload and all raw data generated in this study, including mitochondrial biochemistry, mtDNA content, and blood chemistry, cell counts from CBC and flow cytometry, and de-identified participant information. Requests for resources or other information should be directed to and will be fulfilled by the corresponding author.

Acknowledgements

Work of the authors is supported by the Wharton Fund and NIH grants MH119336, GM119793, MH122706, AG066828, AG056635, AG026307, and UL1TR001873. These studies used the resources of the Irving Cancer Center Core Facility funded in part through center grant P30CA013696.

Author contributions

C.T., R.G.R., K.R.K., S.H., and M.P. designed research. S.R., C.T. and A.M. recruited participants. S.R., M.A.M., and W.W. processed samples and collected data. S.R., C.T, A.J., S.C.S, R.G.R. analyzed and interpreted data. S.R. and M.P. drafted the manuscript. All authors edited and commented on the final version of the manuscript.

References

1. Picard M, Wallace DC, Burelle Y. The rise of mitochondria in medicine. *Mitochondrion*. 2016/09/01/ 2016;30:105-116. doi:10.1016/j.mito.2016.07.003

2. Jang JY, Blum A, Liu J, Finkel T. The role of mitochondria in aging. *The Journal of Clinical Investigation*. 08/31/ 2018;128(9):3662-3670. doi:10.1172/JCI120842

3. Wallace Douglas C. Mitochondrial DNA Variation in Human Radiation and Disease. *Cell*. 2015;163(1):33-38. doi:10.1016/j.cell.2015.08.067

4. Picard M, Trumpff C, Burelle Y. Mitochondrial psychobiology: foundations and applications. *Curr Opin Behav Sci*. 2019/08/01/ 2019;28:142-151. doi:10.1016/j.cobeha.2019.04.015

5. Chacko BK, Kramer PA, Ravi S, et al. Methods for defining distinct bioenergetic profiles in platelets, lymphocytes, monocytes, and neutrophils, and the oxidative burst from human blood. *Lab Invest*. 2013;93(6):690-700. doi:10.1038/labinvest.2013.53

6. Weiss SL, Selak MA, Tuluc F, et al. Mitochondrial dysfunction in peripheral blood mononuclear cells in pediatric septic shock. *Pediatr Crit Care Med*. 2015;16(1):e4-e12. doi:10.1097/PCC.0000000000000277

7. Karabatsiakis A, Böck C, Salinas-Manrique J, et al. Mitochondrial respiration in peripheral blood mononuclear cells correlates with depressive subsymptoms and severity of major depression. *Translational Psychiatry*. 2014/06/01 2014;4(6):e397-e397. doi:10.1038/tp.2014.44

8. Dixon N, Li T, Marion B, et al. Pilot study of mitochondrial bioenergetics in subjects with acute porphyrias. *Mol Genet Metab*. Nov 2019;128(3):228-235. doi:10.1016/j.ymgme.2019.05.010

9. Ehinger JK, Morota S, Hansson MJ, Paul G, Elmér E. Mitochondrial Respiratory Function in Peripheral Blood Cells from Huntington's Disease Patients. *Mov Disord Clin Pract*. 2016;3(5):472-482. doi:10.1002/mdc3.12308

10. Picard M, Prather AA, Puterman E, et al. A Mitochondrial Health Index Sensitive to Mood and Caregiving Stress. *Biol Psychiatry*. Jul 1 2018;84(1):9-17. doi:10.1016/j.biopsych.2018.01.012

11. Tyrrell DJ, Bharadwaj MS, Van Horn CG, Marsh AP, Nicklas BJ, Molina AJ. Blood-cell bioenergetics are associated with physical function and inflammation in overweight/obese older adults. *Exp Gerontol*. Oct 2015;70:84-91. doi:10.1016/j.exger.2015.07.015

12. Dhabhar FS, Miller AH, Stein M, McEwen BS, Spencer RL. Diurnal and Acute Stress-Induced Changes in Distribution of Peripheral Blood Leukocyte Subpopulations. *Brain, Behavior, and Immunity*. 1994/03/01/ 1994;8(1):66-79. doi:10.1006/brbi.1994.1006

13. Ackermann K, Revell VL, Lao O, Rombouts EJ, Skene DJ, Kayser M. Diurnal rhythms in blood cell populations and the effect of acute sleep deprivation in healthy young men. *Sleep*. Jul 1 2012;35(7):933-40. doi:10.5665/sleep.1954

14. Dhabhar FS, Malarkey WB, Neri E, McEwen BS. Stress-induced redistribution of immune cells--from barracks to boulevards to battlefields: a tale of three hormones--Curt Richter Award winner. *Psychoneuroendocrinology*. Sep 2012;37(9):1345-68. doi:10.1016/j.psyneuen.2012.05.008

15. Beis D, von Känel R, Heimgartner N, et al. The Role of Norepinephrine and α-Adrenergic Receptors in Acute Stress-Induced Changes in Granulocytes and Monocytes. *Psychosom Med*. Sep 2018;80(7):649-658. doi:10.1097/psy.0000000000000620

16. Patin E, Hasan M, Bergstedt J, et al. Natural variation in the parameters of innate immune cells is preferentially driven by genetic factors. *Nature Immunology*. 2018/03/01 2018;19(3):302-314. doi:10.1038/s41590-018-0049-7

17. Pyle A, Burn DJ, Gordon C, Swan C, Chinnery PF, Baudouin SV. Fall in circulating mononuclear cell mitochondrial DNA content in human sepsis. *Intensive Care Medicine*. 2010/06/01 2010;36(6):956-962. doi:10.1007/s00134-010-1823-7

18. Maianski NA, Geissler J, Srinivasula SM, Alnemri ES, Roos D, Kuijpers TW. Functional characterization of mitochondria in neutrophils: a role restricted to apoptosis. *Cell Death Differ*. Feb 2004;11(2):143-53. doi:10.1038/sj.cdd.4401320

19. Kramer PA, Ravi S, Chacko B, Johnson MS, Darley-Usmar VM. A review of the mitochondrial and glycolytic metabolism in human platelets and leukocytes: implications for their use as bioenergetic biomarkers. *Redox Biol*. 2014;2:206-10. doi:10.1016/j.redox.2013.12.026

20. Butler LM, Metson-Scott T, Felix J, et al. Sequential adhesion of platelets and leukocytes from flowing whole blood onto a collagen-coated surface: requirement for a GpVI-binding site in collagen. *Thromb Haemost*. May 2007;97(5):814-21.

21. Hurtado-Roca Y, Ledesma M, Gonzalez-Lazaro M, et al. Adjusting MtDNA Quantification in Whole Blood for Peripheral Blood Platelet and Leukocyte Counts. *PLOS ONE*. 2016;11(10):e0163770. doi:10.1371/journal.pone.0163770

22. Banas B, Kost BP, Goebel FD. Platelets, a typical source of error in real-time PCR quantification of mitochondrial DNA content in human peripheral blood cells. *Eur J Med Res*. Aug 31 2004;9(8):371-7.

23. Urata M, Koga-Wada Y, Kayamori Y, Kang D. Platelet contamination causes large variation as well as overestimation of mitochondrial DNA content of peripheral blood mononuclear cells. *Ann Clin Biochem*. Sep 2008;45(Pt 5):513-4. doi:10.1258/acb.2008.008008

24. Shim HB, Arshad O, Gadawska I, Côté HCF, Hsieh AYY. Platelet mtDNA content and leukocyte count influence whole blood mtDNA content. *Mitochondrion*. Mar 7 2020;52:108-114. doi:10.1016/j.mito.2020.03.001

25. Pagliarini DJ, Calvo SE, Chang B, et al. A mitochondrial protein compendium elucidates complex I disease biology. *Cell*. Jul 11 2008;134(1):112-23. doi:10.1016/j.cell.2008.06.016

26. Fecher C, Trovò L, Müller SA, et al. Cell-type-specific profiling of brain mitochondria reveals functional and molecular diversity. *Nature Neuroscience*. 2019/10/01 2019;22(10):1731-1742. doi:10.1038/s41593-019-0479-z

27. Picard M, Hepple RT, Burelle Y. Mitochondrial functional specialization in glycolytic and oxidative muscle fibers: tailoring the organelle for optimal function. *Am J Physiol Cell Physiol*. Feb 15 2012;302(4):C629-41. doi:10.1152/ajpcell.00368.2011

28. Pearce EL, Poffenberger MC, Chang C-H, Jones RG. Fueling Immunity: Insights into Metabolism and Lymphocyte Function. *Science*. 2013;342(6155):1242454. doi:10.1126/science.1242454

29. Nomura M, Liu J, Rovira II, et al. Fatty acid oxidation in macrophage polarization. *Nature immunology*. 2016;17(3):216-217. doi:10.1038/ni.3366

30. Michalek RD, Gerriets VA, Jacobs SR, et al. Cutting edge: distinct glycolytic and lipid oxidative metabolic programs are essential for effector and regulatory CD4+ T cell subsets. *J Immunol*. 2011;186(6):3299-3303. doi:10.4049/jimmunol.1003613

31. Jones N, Vincent EE, Cronin JG, et al. Akt and STAT5 mediate naïve human CD4+ T-cell early metabolic response to TCR stimulation. *Nature Communications*. 2019/05/03 2019;10(1):2042. doi:10.1038/s41467-019-10023-4

32. Brand K. Glutamine and glucose metabolism during thymocyte proliferation. Pathways of glutamine and glutamate metabolism. *Biochem J*. 1985;228(2):353-361. doi:10.1042/bj2280353

33. Ron-Harel N, Ghergurovich JM, Notarangelo G, et al. T Cell Activation Depends on Extracellular Alanine. *Cell Rep*. 2019/09// 2019;28(12):3011-3021.e4. doi:10.1016/j.celrep.2019.08.034

34. Bektas A, Schurman SH, Gonzalez-Freire M, et al. Age-associated changes in human CD4(+) T cells point to mitochondrial dysfunction consequent to impaired autophagy. *Aging (Albany NY)*. Nov 9 2019;11(21):9234-9263. doi:10.18632/aging.102438

35. Picard M, McEwen BS. Psychological Stress and Mitochondria: A Systematic Review. *Psychosom Med*. Feb/Mar 2018;80(2):141-153. doi:10.1097/psy.0000000000000545

36. Gan Z, Fu T, Kelly DP, Vega RB. Skeletal muscle mitochondrial remodeling in exercise and diseases. *Cell Research*. 2018/10/01 2018;28(10):969-980. doi:10.1038/s41422-018-0078-7

37. Nikolich-Žugich J. Aging of the T cell compartment in mice and humans: from no naive expectations to foggy memories. *J Immunol*. 2014;193(6):2622-2629. doi:10.4049/jimmunol.1401174

38. Larsen S, Nielsen J, Hansen CN, et al. Biomarkers of mitochondrial content in skeletal muscle of healthy young human subjects. *J Physiol*. 2012;590(14):3349-3360. doi:10.1113/jphysiol.2012.230185

39. Biino G, Santimone I, Minelli C, et al. Age- and sex-related variations in platelet count in Italy: a proposal of reference ranges based on 40987 subjects' data. *PloS one*. 2013;8(1):e54289-e54289. doi:10.1371/journal.pone.0054289

40. Zhang J, Li M, He Y. Large population study for age- and gender- related variations of platelet indices in Southwest China healthy adults. *Hematology & Transfusion International Journal*. 2015;1

41. Verhoeven JE, Révész D, Picard M, et al. Depression, telomeres and mitochondrial DNA: between- and within-person associations from a 10-year longitudinal study. *Mol Psychiatry*. Apr 2018;23(4):850-857. doi:10.1038/mp.2017.48

42. Mengel-From J, Thinggaard M, Dalgård C, Kyvik KO, Christensen K, Christiansen L. Mitochondrial DNA copy number in peripheral blood cells declines with age and is associated with general health among elderly. *Hum Genet*. Sep 2014;133(9):1149-59. doi:10.1007/s00439-014-1458-9

43. Zhang R, Wang Y, Ye K, Picard M, Gu Z. Independent impacts of aging on mitochondrial DNA quantity and quality in humans. *BMC Genomics*. 2017/11/21 2017;18(1):890. doi:10.1186/s12864-017-4287-0

44. Nicoli F, Papagno L, Frere JJ, et al. Naïve CD8+ T-Cells Engage a Versatile Metabolic Program Upon Activation in Humans and Differ Energetically From Memory CD8+ T-Cells. Original Research. *Frontiers in Immunology*. 2018-December-21 2018;9(2736)doi:10.3389/fimmu.2018.02736

45. van der Windt GJW, O'Sullivan D, Everts B, et al. CD8 memory T cells have a bioenergetic advantage that underlies their rapid recall ability. *Proceedings of the National Academy of Sciences*. 2013;110(35):14336. doi:10.1073/pnas.1221740110

46. van der Windt GJ, Everts B, Chang CH, et al. Mitochondrial respiratory capacity is a critical regulator of CD8+ T cell memory development. *Immunity*. Jan 27 2012;36(1):68-78. doi:10.1016/j.immuni.2011.12.007

47. Iershov A, Nemazanyy I, Alkhoury C, et al. The class 3 PI3K coordinates autophagy and mitochondrial lipid catabolism by controlling nuclear receptor PPARα. *Nature Communications*. 2019/04/05 2019;10(1):1566. doi:10.1038/s41467-019-09598-9

48. Turner N, Bruce CR, Beale SM, et al. Excess lipid availability increases mitochondrial fatty acid oxidative capacity in muscle: evidence against a role for reduced fatty acid oxidation in lipid-induced insulin resistance in rodents. *Diabetes*. Aug 2007;56(8):2085-92. doi:10.2337/db07-0093

49. Lindquist C, Bjørndal B, Rossmann CR, Svardal A, Hallström S, Berge RK. A fatty acid analogue targeting mitochondria exerts a plasma triacylglycerol lowering effect in rats with impaired carnitine biosynthesis. *PLoS One*. 2018;13(3):e0194978. doi:10.1371/journal.pone.0194978

50. Picard M, Jung B, Liang F, et al. Mitochondrial dysfunction and lipid accumulation in the human diaphragm during mechanical ventilation. *Am J Respir Crit Care Med*. Dec 1 2012;186(11):1140-9. doi:10.1164/rccm.201206-0982OC

51. Karan KR, Trumpff C, McGill MA, et al. Mitochondrial respiratory capacity modulates LPS-induced inflammatory signatures in human blood. *Brain, Behavior, & Immunity - Health*. 2020/05/01/ 2020;5:100080. doi:10.1016/j.bbih.2020.100080

52. Artyomov MN, Van den Bossche J. Immunometabolism in the Single-Cell Era. *Cell Metabolism*. 2020/10/06/ 2020;doi:10.1016/j.cmet.2020.09.013

53. Segerstrom SC, Sephton SE, Westgate PM. Intraindividual variability in cortisol: Approaches, illustrations, and recommendations. *Psychoneuroendocrinology*. 2017/04/01/ 2017;78:114-124. doi:10.1016/j.psyneuen.2017.01.026

54. Ventura-Clapier R, Piquereau J, Veksler V, Garnier A. Estrogens, Estrogen Receptors Effects on Cardiac and Skeletal Muscle Mitochondria. Review. *Frontiers in Endocrinology*. 2019-August-14 2019;10(557)doi:10.3389/fendo.2019.00557

55. Silaidos C, Pilatus U, Grewal R, et al. Sex-associated differences in mitochondrial function in human peripheral blood mononuclear cells (PBMCs) and brain. *Biology of Sex Differences*. 2018/07/25 2018;9(1):34. doi:10.1186/s13293-018-0193-7

56. Short KR, Bigelow ML, Kahl J, et al. Decline in skeletal muscle mitochondrial function with aging in humans. *Proc Natl Acad Sci U S A*. Apr 12 2005;102(15):5618-23. doi:10.1073/pnas.0501559102

57. Hebert SL, Marquet-de Rougé P, Lanza IR, et al. Mitochondrial Aging and Physical Decline: Insights From Three Generations of Women. *J Gerontol A Biol Sci Med Sci*. 2015/11// 2015;70(11):1409-1417. doi:10.1093/gerona/glv086

58. Wachsmuth M, Hübner A, Li M, Madea B, Stoneking M. Age-Related and Heteroplasmy-Related Variation in Human mtDNA Copy Number. *PLOS Genetics*. 2016;12(3):e1005939. doi:10.1371/journal.pgen.1005939

59. Moore AZ, Ding J, Tuke MA, et al. Influence of cell distribution and diabetes status on the association between mitochondrial DNA copy number and aging phenotypes in the InCHIANTI study. *Aging Cell*. 2018;17(1):e12683. doi:10.1111/acel.12683

60. Ye K, Lu J, Ma F, Keinan A, Gu Z. Extensive pathogenicity of mitochondrial heteroplasmy in healthy human individuals. *Proceedings of the National Academy of Sciences*. 2014;111(29):10654. doi:10.1073/pnas.1403521111

61. Giordano C, Iommarini L, Giordano L, et al. Efficient mitochondrial biogenesis drives incomplete penetrance in Leber's hereditary optic neuropathy. *Brain*. 2014;137(Pt 2):335-353. doi:10.1093/brain/awt343

62. Yu-Wai-Man P, Sitarz KS, Samuels DC, et al. OPA1 mutations cause cytochrome c oxidase deficiency due to loss of wild-type mtDNA molecules. *Hum Mol Genet*. 2010;19(15):3043-3052. doi:10.1093/hmg/ddq209

63. Nicholls DG, Ferguson SJ. *Bioenergetics*. Academic Press; 2013.

64. Hernansanz-Agustín P, Enríquez JA. Generation of Reactive Oxygen Species by Mitochondria. *Antioxidants (Basel)*. 2021;10(3):415. doi:10.3390/antiox10030415

65. Brand MD, Chen CH, Lehninger AL. Stoichiometry of H+ ejection during respiration-dependent accumulation of Ca2+ by rat liver mitochondria. *Journal of Biological Chemistry*. 1976/02/25/ 1976;251(4):968-974. doi:10.1016/S0021-9258(17)33787-0

66. Martínez-Reyes I, Diebold LP, Kong H, et al. TCA Cycle and Mitochondrial Membrane Potential Are Necessary for Diverse Biological Functions. *Mol Cell*. Jan 21 2016;61(2):199-209. doi:10.1016/j.molcel.2015.12.002

67. Picard M, Zhang J, Hancock S, et al. Progressive increase in mtDNA 3243A>G heteroplasmy causes abrupt transcriptional reprogramming. *Proc Natl Acad Sci U S A*. Sep 23 2014;111(38):E4033-42. doi:10.1073/pnas.1414028111

68. Field CS, Baixauli F, Kyle RL, et al. Mitochondrial Integrity Regulated by Lipid Metabolism Is a Cell-Intrinsic Checkpoint for Treg Suppressive Function. *Cell Metab*. Feb 4 2020;31(2):422-437.e5. doi:10.1016/j.cmet.2019.11.021

Supplemental Methods and Procedures

This document is an extended version of the Methods section in the main text, with additional technical details to facilitate the reproducibility of all parts of this study.

Blood Collection

*A total o*f 100 ml of blood was drawn from the antecubital vein for each participant and included one EDTA tube (Cat# BD367841, 2 ml) for complete blood count (CBC), two SST coated tubes (Cat#BD367986, 5 ml) for hormonal measures and blood biochemistry in serum, and 11 Acid Dextrose A (ACD-A) tubes (Cat# BD364606, 8.5 ml) for leukocyte isolation and mitochondrial analyses, in order of collection. All tubes were gently inverted 10-12 times immediately after draw to ensure proper mixing. The EDTA and SST tubes for hematological and blood biochemistry were processed by the Center for Advanced Laboratory Medicine (CALM) Lab, and the ACD-A tubes were further processed for cell isolation.

PBMCs and leukocyte isolation

Ficoll 1077 and 1119 (Sigma), Hanks Balanced Salt Sodium (HBSS) without phenol red, calcium and magnesium (Life Technologies, Cat# 14175103) supplemented with 2% BSA (Sigma, Cat# A9576) (HBSS/BSA), HBSS/BSA supplemented with 1 mM of EDTA (Sigma, Cat# E9884) (HBSS/BSA/EDTA), and FBS (Thermofisher, cat# 10437036) were brought to room temperature overnight. PBMCs were isolated on 15 ml of low density Ficoll 1077 in a 50 ml conical tube, and total leukocytes were separated on 15ml of higher density Ficoll 1119 distributed across 7 conical tubes. Blood was first pooled and diluted with HBSS/BSA in a 1:1 ratio, and 25 ml of diluted blood was carefully layered on Ficoll and then centrifuged immediately at 700 x g for 30 minutes (no brake) in a horizontal rotor (swing-out head) tabletop centrifuge, at room temperature. Immediately after centrifugation, cells at the interface were collected and washed in 50 ml HBSS/BSA and centrifuged at 700 x g for 10 minutes. Supernatants were discarded and leukocyte pellets washed again in HBSS/BSA/EDTA and centrifuged at 700 x g for 10 minutes to limit platelet contamination. Low concentration EDTA (1mM) was used to prevent cell-cell adhesion or platelet activation, but a higher concentration was not used to avoid perturbing downstream mitochondrial assays.

To perform cell count, both i) PBMCs (1:10 dilution) and ii) total leukocytes (1:100 dilution) were resuspended in 1 ml of HBSS/BSA/EDTA and counted on the Countess II FL

Automated Cell Counter (Thermo Fisher Scientific, Cat# AMQAF1000) in a 1:1 dilution with trypan blue. Counts were performed in duplicates. If the difference between duplicates >10%, the count was repeated and the grand mean of the cell counts taken. Pellets of 5 million PBMCs were aliquoted and frozen at -80ºC for mitochondrial assays.

Immunolabeling of cell surface markers

Two antibody cocktails meant for i) cell counting (Cocktail 1) and ii) cell sorting (Cocktail 2), were prepared for fluorescence-activated cell sorting (FACS) (see Supplemental Table 4 for details). Antibodies were gently mixed, kept at 4°C, and shielded from light to avoid bleaching. Cocktail 1 (containing cell surface markers for activated T lymphocytes) was prepared with 17.5 ul HBSS/BSA/EDTA and 2.5 ul per antibody (13 markers, 32.5 ul total antibody mix), for a total of 50 ul. Cocktail 2 was prepared with 200 ul HBSS/BSA/EDTA and 25 ul per antibody (12 markers, 300 ul total sorting antibody mix), for a total of 500 ul.

Prior to each study visit, cell collection tubes (Cat#: 352063, polypropylene, 5 ml) were coated with 4.5ml of DMEM/10% FBS media to minimize cell-tube adhesion and maximize the recovery of sorted cells. Tubes were incubated for 24 hours at room temperature and stored at 4°C until use, and decanted prior to use. Two coated polypropylene tubes were used for the FACS-ready antibody-labeled leukocytes, and an additional 60 coated polypropylene falcon tubes were decanted and 500 ul of media (DMEM/10% FBS) was added to receive sorted cells.

Prior to immunolabeling, total leukocytes were incubated with blocking buffer (to block non-specific binding to FC receptors) at a 1:10 dilution and incubated at room temperature for 10 minutes. A 2 million cell aliquot was diluted to a final volume of 100 ul with HBSS/BSA/EDTA and combined with 50 ul of Cocktail 1. The remainder of total leukocytes (~100M cells) were incubated with 500 ul of Cocktail 2 for 20 minutes in the dark, at room temperature. Both cell preparations were then washed with 5 ml of HBSS/BSA/EDTA and centrifuged at 700 x g for 5 minutes. Using the propylene tubes, Cocktail 1 cells were resuspended in 200 ul of HBSS/BSA/EDTA, and total leukocytes for FACS were resuspended to final concentration of 20 million cells/ml with HBSS/BSA/EDTA.

Fluorescence-activated cell sorting (FACS)

Cells labeled with the Cocktail 1 (counting) panel was only used for data acquisition and phenotype analysis. Cells labeled with the Cocktail 2 (sorting) panel was FACS sorted using a

BD™ Influx cell sorter to isolate the subpopulations from peripheral blood. The sorter was controlled using BD FACS Sortware. Cells were sorted using 100 um size nozzle and under the sheath pressure of 20 psi. Sorting speed was kept around 11,000-12,000 events/second. Cell concentration for sorting was measured at about $15x10^6$ cells per ml. Cell sorter drop frequency was 37 KHz, stream focus was 10%, maximum drop charge was 110 Volts. A six-way sorting, 1.0 drop pure sort mode was used to sort the cell subpopulations. Stream deflections were -84, -65, -32, 32, 65, and 84 for six-way sort from left to right. For each participant, 1 million cells (Cocktail 1 panel) were run first to calculate the potential yield of each subpopulation, including neutrophils, B lymphocytes, monocytes, NK cells, naïve $CD4^+$ and $CD8^+$, CM $CD4^+$ and $CD8^+$, EM $CD4^+$ and $CD8^+$, and TEMRA $CD4^+$ and $CD8^+$ lymphocytes (total cell number x percentage of each subpopulation). The six most abundant subpopulations were sorted. Purity checks were performed on all sorted subpopulations to ensure the instrument performance was good enough to reach the sorted population purity >95%. Raw data (.fcs file) was exported for further analysis on FCS Express 7 research version.

Processing and storage of sorted cells

Following flow cytometry, sorted cell subtypes were transferred and pooled by pipetting about half of each collection tube (2.5 ml) into larger falcon tubes, gently vortexing to liberate cells that may have adhered to the tube wall, and the remaining volume pipetted into the transfer tube. HBSS/2% BSA was used as necessary to equilibrate and cells were centrifuged at 1,000 x g for 5 minutes. Following centrifugation, each cell pellet was isolated by gently decanting the supernatant and re-suspended into 1ml of HBSS/2% BSA. The resulting purified cell suspensions were transferred to a 1.5 ml Eppendorf tube for each cell type, centrifuged at 2,000 x g for 2 minutes at 4°C, and the supernatant carefully removed to leave a dry cell pellet. Samples were stored in liquid nitrogen for 4-12 months (-170°C) until mitochondrial biochemistry and mtDNAcn analyses were performed as a single batch.

Mitochondrial enzymatic activities

Samples were thawed and homogenized in preparation for enzymatic activity measurements with one tungsten bead and 500 ul of homogenization buffer (1 mM EDTA, 50 mM Triethanolamine). Tubes were transferred to a pre-chilled rack and homogenized using a Tissue Lyser (Qiagen cat# 85300) at 30 cycles/second for 1 minute. Samples were then incubated for 5

minutes at 4°C, and homogenization was repeated for 1 minute and the samples were returned to ice ready for enzymatic assays.

Mitochondrial enzyme activities were quantified spectrophotometrically for citrate synthase (CS), cytochrome c oxidase (COX, Complex IV), succinate dehydrogenase (SDH, Complex II), and NADH dehydrogenase (Complex I) as described previously[10] with minor modifications. Each sample was measured in triplicates for each enzymatic assay (3 wells for total activity and 3 wells for non-specific activity, except for the COX assay where a single non-specific activity value is determined across 30 wells). Homogenate volumes used for each reaction were: CS: 10 ul, COX and SDH: 20 ul, Complex I: 15 ul.

CS activity was measured by detecting the increase in absorbance at 412 nm, in a reaction buffer (200 mM Tris, pH 7.4) containing acetyl-CoA 0.2 mM, 0.2 mM 5,5'- dithiobis-(2-nitrobenzoic acid) (DTNB), 0.55 mM oxaloacetic acid, and 0.1% Triton X-100. Final CS activity was obtained by integrating OD^{412} change from 150-480 sec, and by subtracting the non-specific activity measured in the absence of oxaloacetate. COX activity was measured by detecting the decrease in absorbance at 550 nm, in a 100 mM potassium phosphate reaction buffer (pH 7.5) containing 0.1% n-dodecylmaltoside and 100 μM of purified reduced cytochrome c. Final COX activity was obtained by integrating OD^{550} change over 200-600 sec and by subtracting spontaneous cyt c oxidation without cell lysate. SDH activity was measured by detecting the decrease in absorbance at 600 nm, in potassium phosphate 100 mM reaction buffer (pH 7.5) containing 2 mM EDTA, 1 mg/ml bovine serum albumin (BSA), 4 μM rotenone, 10 mM succinate, 0.25 mM potassium cyanide, 100 μM decylubuquinone, 100 μM DCIP, 200 μM ATP, 0.4 μM antimycin A. Final SDH activity was obtained by integrating OD^{600} change over 200-900 sec and by subtracting activity detected in the presence of malonate (5 mM), a specific inhibitor of SDH. Complex I activity was measured by detecting the decrease in absorbance at 600 nm, in potassium phosphate 100 mM reaction buffer (pH 7.5) containing 2 mM EDTA, 3.5 mg/ml bovine serum albumin (BSA), 0.25 mM potassium cyanide, 100 μM decylubuquinone, 100 μM DCIP, 200 μM NADH, 0.4 μM antimycin A. Final Complex I activity was obtained by integrating OD^{600} change over 120-600 sec and by subtracting activity detected in the presence of rotenone (500 μM) and piericidin A (200 μM), specific inhibitors of Complex I. All assays were performed at 30°C. The

molar extinction coefficients used were 13.6 L $mol^{-1}cm^{-1}$ for DTNB, 29.5 L $mol^{-1}cm^{-1}$ for reduced cytochrome c, and 16.3 L $mol^{-1}cm^{-1}$ for DCIP to transform change in OD into enzyme activity.

Mitochondrial enzymatic activities were measured on a total of 340 samples, including 136 replicates of the same cell type for the same person. This provided more stable estimates of enzymatic activities than single measures would for a total of 204 individual person-cell combinations. The technical variation for each enzyme varied according to cell type, with cell types with lower enzymatic activities generally showing the highest coefficient of variation (C.V.). C.V. averaged across all cell types were: CS = 6.3%, Complex I = 16.6%, SDH = 9.3%, COX = 23.4% (Supplemental Table 3).

Mitochondrial DNA copy number

mtDNAcn was determined as described previously[10] with minor modifications. The same homogenate used for enzymatic measurements (20 ul) was lysed in lysis buffer (100 mM Tris HCl pH 8.5, 0.5% Tween 20, and 200 ug/ml proteinase K) for 10 hours at 55°C followed by inactivation at 95°C for 10 minutes. Five ul of the lysate was directly used as template DNA for measurements of mtDNA copy number. qPCR reactions were set up in triplicates using a liquid handling station (ep-Motion5073, Eppendorf) in 384 well qPCR plates. Duplex qPCR reactions with Taqman chemistry were used to simultaneously quantify mitochondrial and nuclear amplicons in the same reactions. *Master Mix$_1$* for ND1 (mtDNA) and B2M (nDNA) included: TaqMan Universal Master mix fast (life technologies #4444964), 300 nM of primers and 100 nM probe (ND1-Fwd: GAGCGATGGTGAGAGCTAAGGT, ND1-Rev: CCCTAAAACCCGCCACATCT, Probe:HEX-CCATCACCCTCTACATCACCGCCC-3IABkFQ.B2M-Fwd:CCAGCAGAGAATGGAAAGTCAA,B2M-Rev: TCTCTCTCCATTCTTCAGTAAGTCAACT, Probe:FAM-ATGTGTCTGGGTTTCATCCATCCGACA-3IABkFQ). *Master Mix$_2$* for COX1 (mtDNA) and RnaseP (nDNA) included: TaqMan Universal Master Mix fast, 300 nM of primers and 100 nM probe (COX1-Fwd: CTAGCAGGTGTCTCCTCTATCT, COX1-Rev: GAGAAGTAGGACTGCTGTGATTAG, Probe: FAM-TGCCATAACCCAATACCAAACGCC-3IABkFQ. RnaseP-Fwd: AGATTTGGACCTGCGAGCG, RnaseP-Rev: GAGCGGCTGTCTCCACAAGT, Probe: FAM-TTCTGACCTGAAGGCTCTGCGCG-3IABkFQ. The samples were then cycled in a QuantStudio

7 flex qPCR instrument (Applied Biosystems Cat# 4485701) at 50°C for 2 min, 95°C for 20 sec, 95°C for 1 min, 60°C for 20 sec for 40x cycles. Reaction volumes were 20 ul. To ensure comparable Ct values across plates and assays, thresholds for fluorescence detection for both mitochondrial and nuclear amplicons were set to 0.08.

mtDNAcn was calculated using the ΔCt method. The ΔCt was obtained by subtracting the average mtDNA Ct values from the average nDNA Ct values for each pair ND1/B2M and COX1/RNaseP. Relative mitochondrial DNA copies are calculated by raising 2 to the power of the ΔCt and then multiplying by 2 to account for the diploid nature of the nuclear genome (mtDNAcn = 2ΔCt x 2). Both ND1 and COX1 yielded highly correlated mtDNAcn and the average of both amplicon pairs was used as mtDNAcn value for each sample. The overall CV across all cell subtypes was 5.1% for mtDNAcn.

Platelet depletion in PBMCs

For this experiment, participants were 9 community-dwelling older adults (mean age = 79, range: 64-89, 4 women and 5 men). The sample included 7 White and 2 African American participants. Exclusion criteria included diseases or disorders affecting the immune system including autoimmune diseases, cancers, immunosuppressive disorders, or chronic, severe infections; chemotherapy or radiation treatment in the 5 years prior to enrollment; unwillingness to undergo venipuncture; immunomodulatory medications including opioids and steroids; or more than two of the following classes of medications: psychotropics, anti-hypertensives, hormones replacement, or thyroid supplements. Participants were recruited from a volunteer subject pool maintained by the University of Kentucky Sanders-Brown Center on Aging. The study was conducted with the approval of the University of Kentucky Institutional Review Board. Blood (20 mL) was collected by venipuncture into heparinized tubes in the morning hours to control for potential circadian variation. PBMCs were isolated from diluted blood by density gradient centrifugation (20 min at 800 x g, brake off) using Histopaque (Sigma, St. Louis, MO). Buffy coats were washed once, and cells were counted using a hemocytometer. PBMCs (20-30M) were cryopreserved in liquid nitrogen in RPMI-1640 (Lonza) + 10% fetal bovine serum (Hyclone) + 10% DMSO (Fisher), until further processing.

For platelet depletion, PBMCs were first thawed at room temperature and centrifuged at 500 x g for 10 minutes. The supernatant was discarded, and the cells were resuspended in 2 ml of

Hank's Balanced Salt Sodium (HBSS) without phenol red, calcium and magnesium (Life Technologies, Cat#14175103). Cells were then counted on the Countess II FL Automated Cell Counter (Thermo Fisher Scientific, Cat# AMQAF1000) in a 1:1 dilution with trypan blue. Cells were then divided into 2 aliquots: 1) 10 million cells for total PBMCs; 2) 11 million cells for platelet depletion. The total PBMCs were centrifuged at 2,000 x g for 2 min at 4ºC and subsequently frozen as a dry pellet at -80ºC until processing for enzymatic assays and qPCR. The PBMCs destined for platelet deletion cells were processed immediately.

The total PBMCs cell preparation was first immunolabeled with magnetically-coupled antibodies against the platelet marker CD61. The 11 million platelet-depleted PBMCs were then centrifuged at 300 x g for 10 minutes. After spin, the supernatant was aspirated and cells were resuspended in 80 ul of HBSS. Then 20 ul of the CD61 MicroBeads (Miltenyi Biotec, Cat# 130-051-101) were added to the cells and incubated for 15 minutes at 4ºC to magnetically label platelets. Cells were washed with 2 ml of HBSS and centrifuged at 300 x g for 10 minutes. The LS column (Miltenyi Biotec, Cat# 130-042-401) was placed in the magnetic field of the MACS Separator (Miltenyi Biotec, Cat# 130-091-051). The LS column was equilibrated with HBSS, cells resuspended in 500 ul of HBSS were applied to the LS column, and the CD61- cells were flown through the column and collected in a 15 ml collection tube. The LS column was then washed 3x with 500 ul of HBSS. The flow through was then spun at 500 x g for 10 minutes, the cell pellet was resuspended in 2 ml of HBSS and re-counted to isolate 10 M platelet-depleted cells. These cells were pelleted at 2,000 x g for 10 minutes at 4ºC, the supernatant removed, and cell pellet stored at -80ºC. The platelets ($CD61^{+}$) were recovered by flushing 1 ml of HBSS though the LS column with the plunger in a new tube, centrifuged at 3,000 x g for 10 minutes, the supernatant removed, and the cell pellet stored at -80ºC until all samples could be processed for enzymatic activity assays as a single batch. For each participant, this experiment yielded three samples: 1) total PBMCs, 2) platelet depleted PBMCs, and 3) enriched platelets. Each sample was processed in parallel for RC enzymatic activity assays and mtDNAcn as described above.

Statistical analyses

To adjust for potential order effects across the 340 samples (31 samples per 96-well plate, 17 plates total) a linear adjustment was applied to raw values enzymatic activity measures, which adjusts for potential storage and batch effects, ensuring consistency between the first and last

samples assayed. Samples from both the cohort and repeat participant were processed and analyzed as a single batch.

Mann-Whitney T tests were used to compare sex differences in cell type proportions and mitochondrial measures. Throughout, effect sizes between groups were computed as Hedges' g (g) to quantify the magnitude of group differences in cell type proportions and mitochondrial measures (by sex, mitotype cell subtype and inter-individual differences). Spearman's r (r) was used to assess strength of associations between continuous variables such as age and cell proportion or age and mitochondrial measures. To assess to what extent mitochondrial features are correlated across cell subtypes (co-regulation) and to calculate the average correlation across mitotypes, Spearman's r matrixes were first computed and transformed to Fisher's Z', and then averaged before transforming back to Spearman's r ($r_{Z'}$). One-way non-parametric ANOVA Kruskal-Wallis with post-hoc Dunn's multiple comparison tests were used to compare cell type mitochondrial measures in different cell subtypes and PBMCs. Between- and within-person variation were characterized using coefficients of variation (C.V.). The root mean square of successive differences (rMSSD) was computed to quantify the magnitude of variability between successive weeks for repeated measures. Chi-square tests were computed to compare proportion of mitotype indices categories (enzyme activity per CS, enzyme ratios, enzyme per mtDNA, enzyme per mtDNA density, and enzyme per mtDNA relative to mtDNA density) by age (lower vs higher with increased age) and sex (lower vs higher in men). Finally, one-way non-parametric Friedman tests with post hoc Dunn's multiple comparisons were used to compare mitochondrial measures in platelet-depleted PBMCs, enriched platelets PBMCs, and total PBMCs. Statistical analyses were performed with Prism 8 (GraphPad, CA), R version 4.0.2 and RStudio version 1.3.1056. Statistical significance was set at $p<0.05$.